Formation Evaluation Through Casing 11

Tools and Techniques Available

A number of tools are available for formation evaluation through tubing and casing. They include:

1. Measurements of formation resistivity through casing
2. Passive detection of natural gamma radiation from the formation
3. Neutron logging to detect the thermal-neutron flux returning from the formation after neutron bombardment from a chemical source
4. Pulsed neutron logging
5. Elemental concentration logging

Resistivity Through Casing

Tools to measure formation resistivity through casing are now available. These tools require that any tubing in the well be pulled prior to running the resistivity logging tool into the hole. They are equipped with a number of electrode pads that are forced against the inside of the casing once the tool reaches the bottom of the hole or the depth from which the log is to be attempted. If good physical and electric contact can be maintained between the pads and the casing then a reasonable measurement of the formation resistivity behind the casing may be obtained.

The operating principal relies on the fact that while the majority of any current flowing will be "short circuited" by the conductive casing itself a minute portion will in fact "leak off" and be detectable by measurement of the minute voltage difference between the tool and "ground" electrode located at surface. The principal is illustrated in Fig. 11.1.

The logical application of resistivity through casing measurements is in old wells where either no resistivity log is available or where a comparison can be made between original and the current formation resistivities. Potential benefits include detection of bypassed pay zones and/or mapping of fluid contact changes with time.

R.M. Bateman, *Cased-Hole Log Analysis and Reservoir Performance Monitoring*,
DOI 10.1007/978-1-4939-2068-6_11

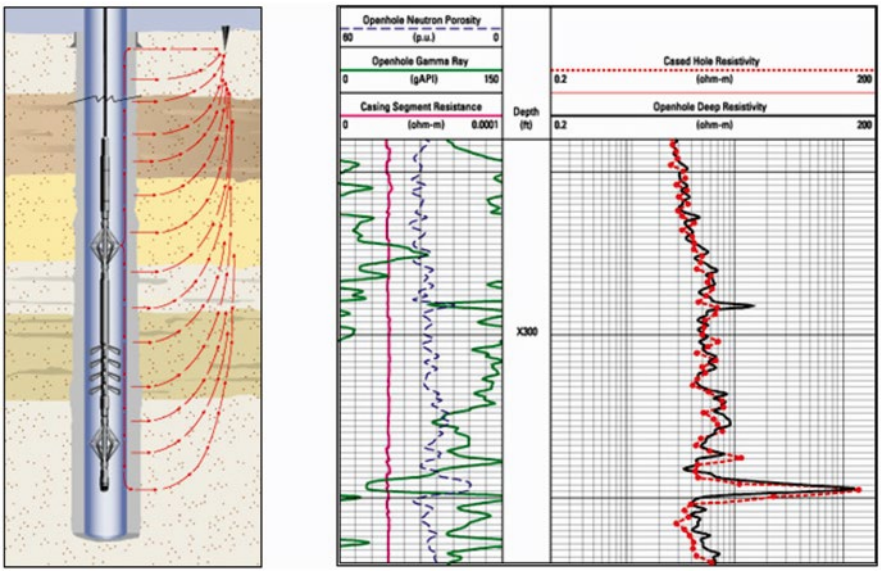

Fig. 11.1 Measurement of formation resistivity through casing

The Gamma Ray Log

Gamma ray logs are used for four main purposes:

1. Correlation and depth positioning
2. Evaluation of the shale content of a formation
3. Mineral analysis
4. Monitoring of radioactive salts deposited on tubulars

The gamma ray log measures the natural gamma ray emissions from subsurface formations. Since gamma rays can pass through steel casing, measurements can be made in both open and cased holes. In other applications, induced gamma rays are measured. These may be γ-rays of capture as used in pulsed neutron logging, or γ-rays produced by inelastic neutron interaction with nuclei in the formation. These latter are used to identify the formation elemental concentrations. These will be discussed later in this chapter.

Figure 11.2 shows a typical gamma ray log. It is normally presented in Track 1 on a linear grid and is scaled in API units, which will be defined later. On this grid, gamma ray activity increases from left to right. Modern gamma ray tools are in the form of double-ended subs that can be sandwiched into practically any logging tool string; thus, the gamma ray can be run with practically any tool available.

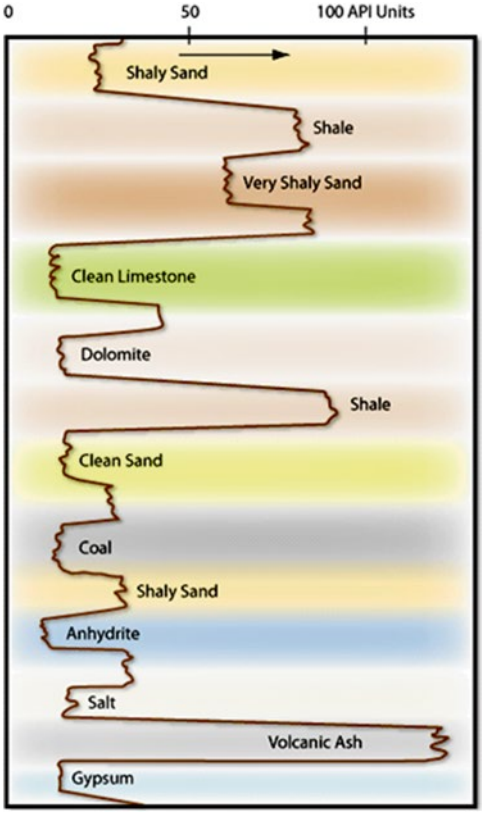

Fig. 11.2 Gamma ray log presentation

Origin of Natural Gamma Rays

Gamma rays originate from three sources in nature: the radioactive elements in the Uranium and Thorium groups, and Potassium. Uranium^{235}, Uranium^{238}, and Thorium^{232} all decay, via a long chain of daughter products, to stable lead isotopes. An isotope of Potassium, K^{40}, decays to Argon, giving off a gamma ray as shown in Fig. 11.3.

Note that each type of decay is characterized by a gamma ray of a specific energy (wave length) and that the frequency of occurrence for each specific energy level is different. Figure 11.4 shows this relationship between gamma ray energy and frequency of occurrence. This is an important concept, since it is used as the basis for measurement in the natural gamma spectroscopy tools.

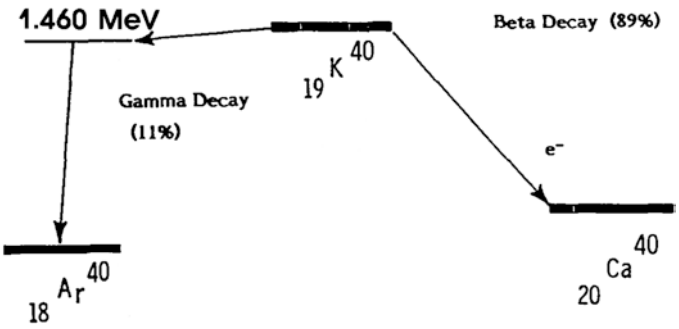

Fig. 11.3 Decay scheme of $_{19}K^{40}$

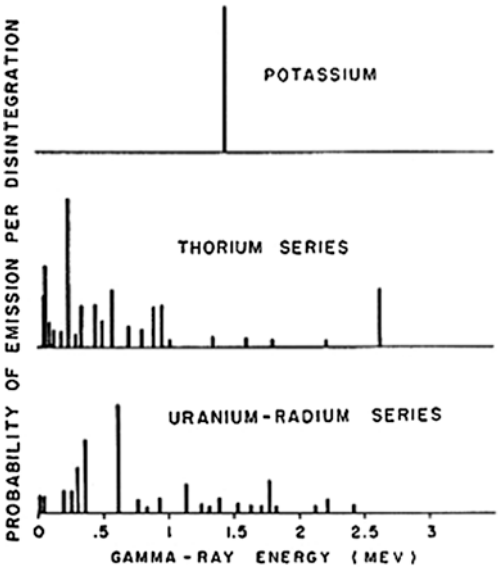

Fig. 11.4 Gamma ray emission spectra of radioactive minerals

Abundance of Naturally Occurring Radioactive Minerals

An average shale contains 6 ppm Uranium, 12 ppm Thorium, and 2 % Potassium. Since the various gamma ray sources are not all equally effective, it is more informative to consider this mix of radioactive materials on a common basis, for example, by reference to Potassium equivalents (i.e., the amount of Potassium that would produce the same number of gamma rays per unit of time). Reduced to a common denominator, the average shale contains Uranium equivalent to 4.3 % Potassium, Thorium equivalent to 3.5 % Potassium, and 2 % Potassium. An *average* shale is hard to find.

Shale is a mixture of clay minerals, sand, silts, and other extraneous materials; thus, there can be no "standard" gamma ray activity for shale. Indeed, the main clay minerals vary enormously in their natural radioactivity. Kaolinite has no Potassium, whereas Illite contains between 4 and 8 % Potassium. Montmorillonite contains less than 1 % Potassium. Occasionally, natural radioactivity may be due to the presence of dissolved Potassium or other salts in the water contained in the pores of the shale.

Operating Principle of Gamma ray Tools

Gamma ray tools consist of a gamma ray detector and the associated electronics for passing the gamma ray count rate to the surface. Traditionally, two types of gamma ray detectors have been used in the logging industry: Geiger-Müeller and scintillation detectors. Today, practically all gamma ray tools use scintillation detectors containing a sodium iodide crystal[1] (Fig. 11.5). When a gamma ray strikes the crystal, a single photon of light is emitted. This tiny flash of light then strikes a photo cathode made from cesium antimony or silver magnesium. Each photon, when hitting the photo cathode, releases a bundle of electrons. These in turn are accelerated in an electric field to strike another electrode producing an even bigger bundle (a shower) of electrons. This process is repeated through a number of stages until a final electrode conducts a small current through a measure resistor to give a voltage pulse that signals that a gamma ray struck the sodium iodide crystal. The system has a very short dead time and can register many counts per second without becoming swamped by numerous simultaneous signals.

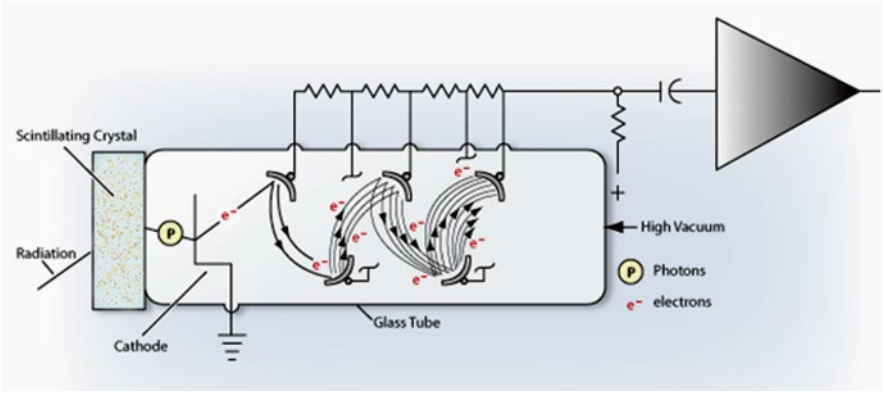

Fig. 11.5 Scintillation counter. Courtesy Halliburton

[1] Sodium Iodide (NaI) and Cesium Iodide (CsI) crystal detectors have relatively poor resolution. Modern "High Resolution" GR logging tools now use Barium Germanite (BGO) detectors, which have better resolution. The better resolution yet can be obtained, using intrinsic Germanium (GSO) or Germanium-Iodide (GeI) or Lanthium Halide (LaBr3 - BrilLanCe™) which must be cryogenetically cooled.

Calibration of Gamma Ray Detectors and Logs

One of the problems of gamma ray logging is the choice of a standard calibration system, since all logging companies use counters of different sizes and shapes encased in steel housings with varying characteristics. On very old logs, the scale might be quoted in micrograms of radium per ton of formation. For many reasons this was found to be an unsatisfactory method of calibration for gamma ray logs, so an API standard was devised. A test pit (installed at the University of Houston) contains an "artificial shale," as illustrated in Fig. 11.6. A cylindrical artificial well, 4 ft in diameter and 24 ft deep contains a central 8-ft section consisting of cement mixed with 13-ppm Uranium, 24 ppm Thorium, and 4 % Potassium. On either side of this central section are 8-ft sections of neat Portland cement. This sandwich is cased with 5½″, J55 casing. The API standard defines the difference in gamma ray count rate between the neat cement and the radioactively doped cement as 200 API units. Any logging service company may place its gamma ray tool in this pit to make a calibration. Field calibration is performed using a portable jig that contains a radioactive pill. The pill typically might be a low activity radium 226 source (e.g., 0.1 milli-curie). When placed at a known radial distance from the center of the gamma ray detector, it produces a known increase over the background count rate. This increase is equivalent to a known number of API units, depending on the tool type and size and the counter it encloses.

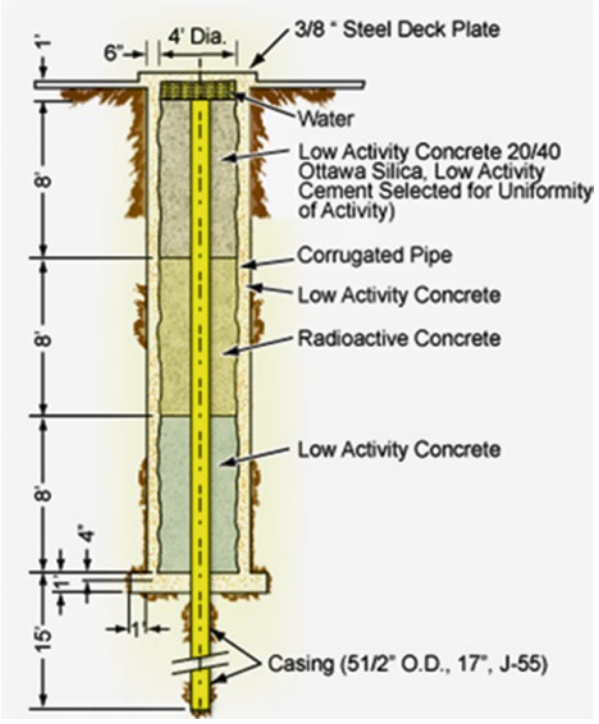

Fig. 11.6 API Gamma Ray Test Pit at the University of Houston

Time Constants

All radioactive processes are subject to statistical variations. For example, if a source of gamma rays emits an average of 100 gamma rays each second over a period of hours, the source will emit 360,000 gamma rays per hour (100/s × 60 s × 60 min). However, if the count is measured for 1 s, the actual count might be less than 100 or more than 100. Thus, a choice must be made. Gamma rays can be counted for a very short interval of time, resulting in a poor estimate of the real count rate; or the gamma rays can be counted for a long time, resulting in a more accurate estimate of the count rate at the expense of an inordinately long time period. In order to average out the statistical variations, various *time constants* may be selected according to the radioactivity level measured. The lower the count rate, the longer the time constant required for adequate averaging of the variations.

In the logging environment, gamma rays can be counted for a short period of time (e.g., 1 s) with the recognition that during that time period, the detector will have moved past the formation whose activity is being measured. Thus, the logging speed and the time interval used to average count rates are interrelated. The following rules of thumb are generally recognized:

Logging speed (ft/h)	Time constant (s)
3,600	1
1,800	2
1,200	3
900	4

At very slow logging speeds (900 ft/h = 1.5 ft/s) and long time constants, a more accurate measurement of absolute activity is obtained at the expense of good bed resolution. At high logging speeds and short time constants, somewhat better bed resolution is obtained at the expense of absolute accuracy. At some future time, when the efficiency of gamma ray detectors and their associated electronics improve by one or two orders of magnitude, the use of a time constant will be obsolete except in the cases of very very inactive formations with intrinsically low gamma ray count rates.

To illustrate this interdependence of logging speed and time constant, Fig. 11.7 shows the same formation logged at two different speeds. On the first run, the logging speed was 80 ft/min and the time constant 1 s. On the second run, the speed was 30 ft/min and the time constant was 2 s. Note the differences in both statistics and bed resolution between the two runs.

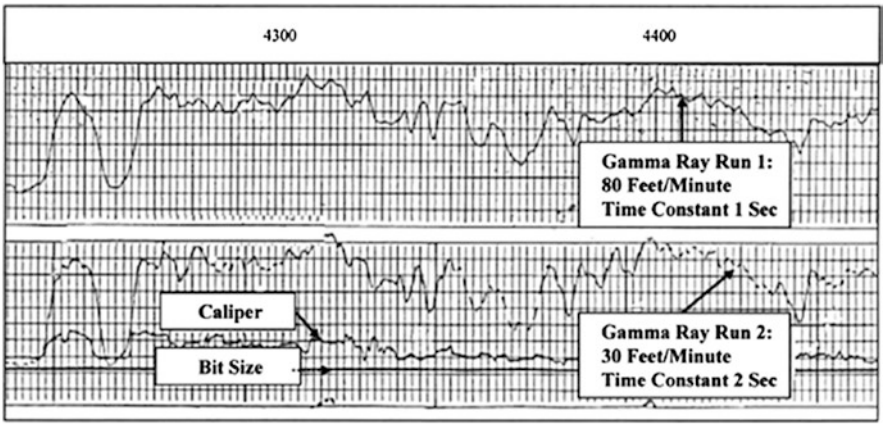

Fig. 11.7 Effects of logging speed and time constant on gamma ray log

Perturbing Effects on Gamma Ray Logs

Gamma ray logs are subject to a number of perturbing effects including:

Sonde position in the hole (centering/eccentering)
Hole size
Mud weight
Casing size and weight
Cement thickness

Since there are innumerable combinations of hole size, mud weights, and tool positions, an arbitrary standard set of conditions is defined as a 3 5/8″ OD tool eccentered in an 8″ hole filled with 10-lb mud. Service company chart books provide analog systems for manually applying corrections but modern logs are almost universally subjected to environmental corrections in real time as the logs are being run that take into account the disturbing effects of temperature, hydrostatic pressure, mud weight, hole and casing size, etc.

Estimating Shale Content from Gamma Ray Logs

Since it is common to find radioactive materials associated with the clay minerals that constitute shales, it is a commonly accepted practice to use the relative gamma ray deflection as a shale-volume indicator. The simplest procedure is to rescale the gamma ray log between its minimum and maximum values from 0 to 100 % shale. A number of studies have shown that this is not necessarily the best method, and alternative relationships have been proposed. To further explain these methods, the

Gamma Ray Index is defined as a linear rescaling of the *GR* log between GR_{min} and GR_{max} such that:

$$\text{Gamma Ray Index} = \frac{GR - GR_{min}}{GR_{max} - GR_{min}}$$

If this index is called *X*, then the alternative relationships can be stated in terms of *X* as follows:

Relationship	Equation
Linear	$V_{sh} = X$
Clavier	$V_{sh} = 1.7 - \sqrt{\left[3.38 - \left(X + 0.7\right)^2\right]}$
Steiber	$V_{sh} = \frac{0.5X}{\left(1.5 - X\right)}$
Bateman	$V_{sh} = X^{(X + \text{GR Factor})}$

where the *GR Factor* is a number chosen to force the result to imitate the behavior of either the Clavier or the Steiber relationship. Figure 11.8 illustrates comparatively the difference between these alternative relationships.

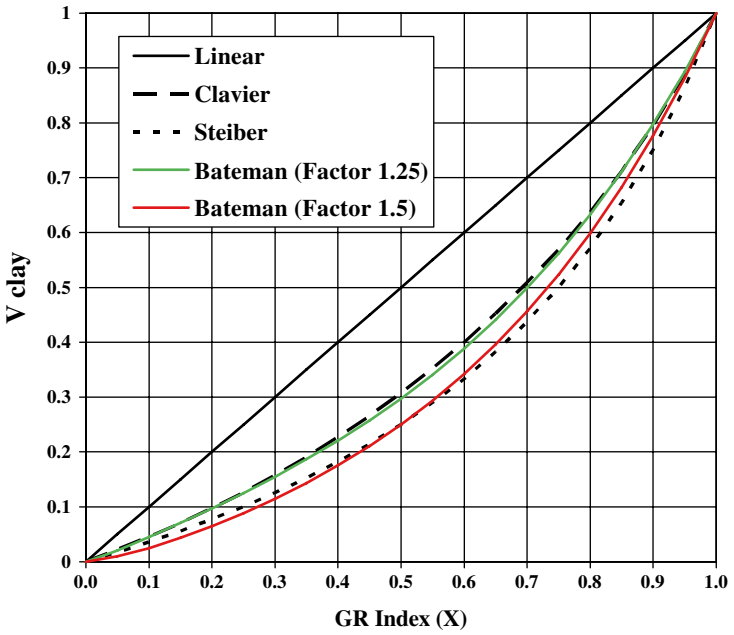

Fig. 11.8 V_{clay} as a function of Gamma Ray Index

Gamma Ray Spectroscopy

Each radioactive decay produces a gamma ray that is unique. These various gamma rays have characteristic energy levels and occur in characteristic abundance, as expressed in counts per time period. The simple method of just counting how many gamma rays a formation produces can be carried a step further to count how many gamma rays from each energy group it produces. The spectrum produced when the number of occurrences is plotted against the energy group is characteristic of the formation logged. Figure 11.9 shows such a spectrum, where energies from 0 to approximately 3 MeV have been split into 256 specific energy bins. The number of gamma rays in each bin is plotted on the *Y*-axis. This spectrum can be thought of as a mixture of the three individual spectra belonging to uranium, thorium, and potassium. Some unique mixture of these three radioactive families would have the same spectrum as the observed one. The trick is to find a quick and easy method of discovering that unique mixture. Fortunately, on-board computers in logging trucks are capable of quickly finding a "best fit" and producing continuous curves showing the concentrations of U, Th, and K.

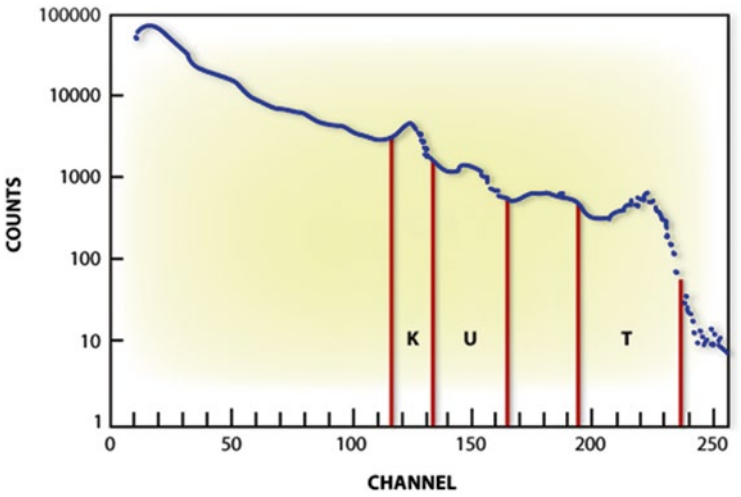

Fig. 11.9 Gamma ray energy spectrum and elemental "windows"

Figure 11.10 illustrates a gamma ray spectral log. Both total gamma ray activity (SGR) and a uranium-free version of the total activity are displayed in Track 1. Units are API. In Tracks 2 and 3, the concentration of U, Th, and K are displayed. Depending on the logging service company, the units may be in counts/s, ppm, or percent.

Question #11.1
In the example shown in Fig. 11.10, determine which element is responsible for the high activity seen on the total gamma ray intensity curve at the point marked A.

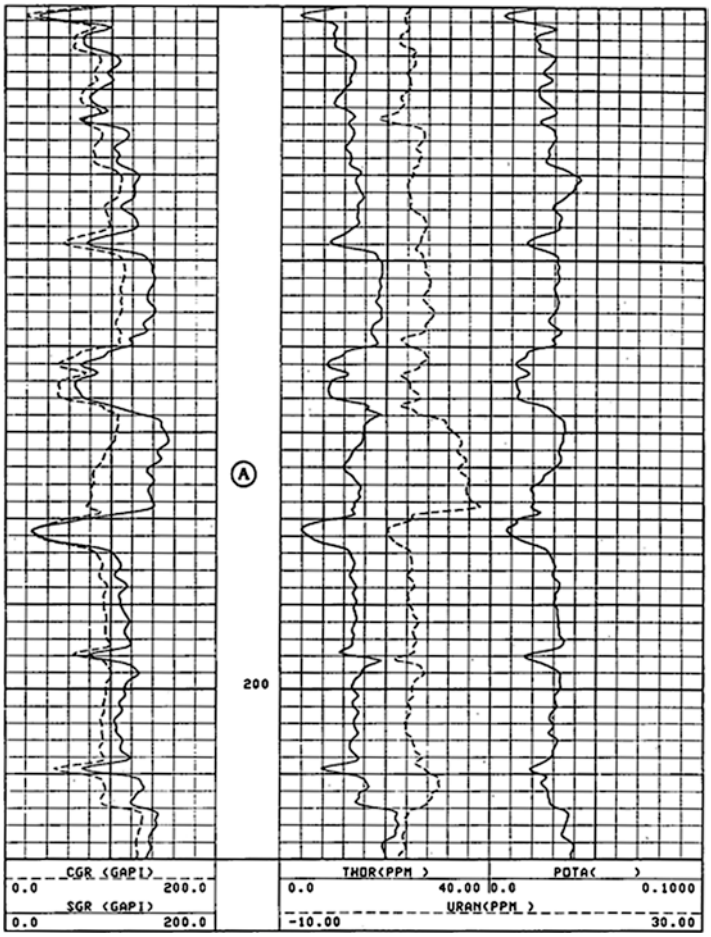

Fig. 11.10 Spectral gamma ray log. Courtesy Schlumberger

Interpretation of Natural Gamma Ray Spectra Logs

Several techniques are in use for the interpretation of natural gamma ray spectra logs. One is the use of the uranium curve as an indicator of fractures. This is more fully described by Fertl et al. More recently the development of unconventional reservoirs has benefited for the presence of uranium in organic shales that may be hydraulically fractured (fracked) and produced. In these formations the uranium content is often related to the total organic carbon (TOC) content of the formation.

Another technique is to apply the U, Th, and K concentrations in combination with other log data to determine lithology and clay type, as described by Marett et al. Still another approach could be called the geochemical method as described by Hassan et al. (1976). Figure 11.11 illustrates the variation of the thorium/potassium ratio in a number of minerals ranging from potassium-feldspar to bauxite.

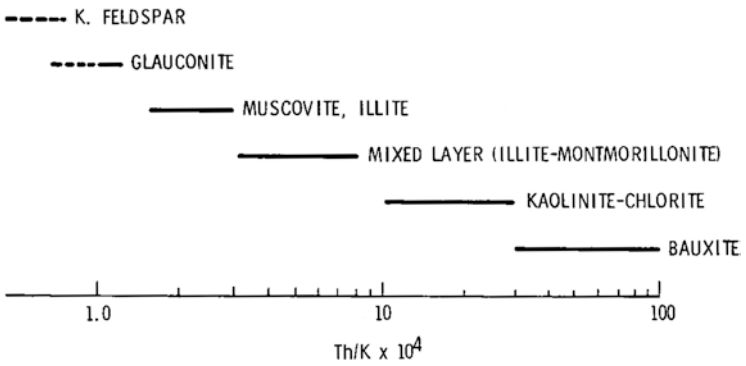

Fig. 11.11 Thorium/Potassium ratios for various minerals. Reprinted by permission of the SPWLA from Hassan et al. 1976. Courtesy Schlumberger

Figure 11.12 maps a number of radioactive minerals as a function of their thorium and potassium content. Other elemental ratios are also useful indicators. For example, a low U/Th ratio indicates reduced black shales. Uranium by itself may indicate a high organic carbon content, which in turn may indicate the presence of gas.

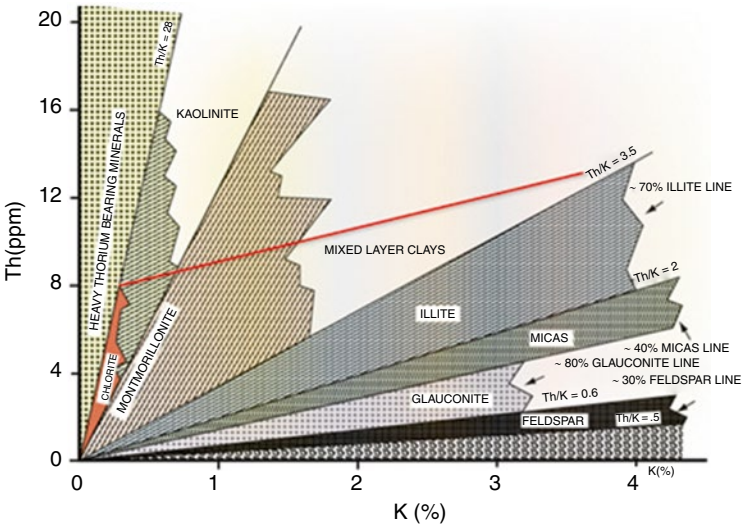

Fig. 11.12 Thorium/Potassium crossplot for minerals identification. Courtesy Schlumberger

Field presentations of gamma ray spectra can assist the analyst in the task of mineral identification by offering curve plots with ratios of the three components (U, Th, and K) already computed. Figure 11.13 gives an example of one such presentation. Track 1 shows total gamma ray together with a uranium-free curve. Track 2 gives three ratios, uranium/potassium, thorium/uranium, and thorium/potassium. Track 3 gives a coded display on which the coded area represents the formations with both the highest potassium and the highest thorium content.

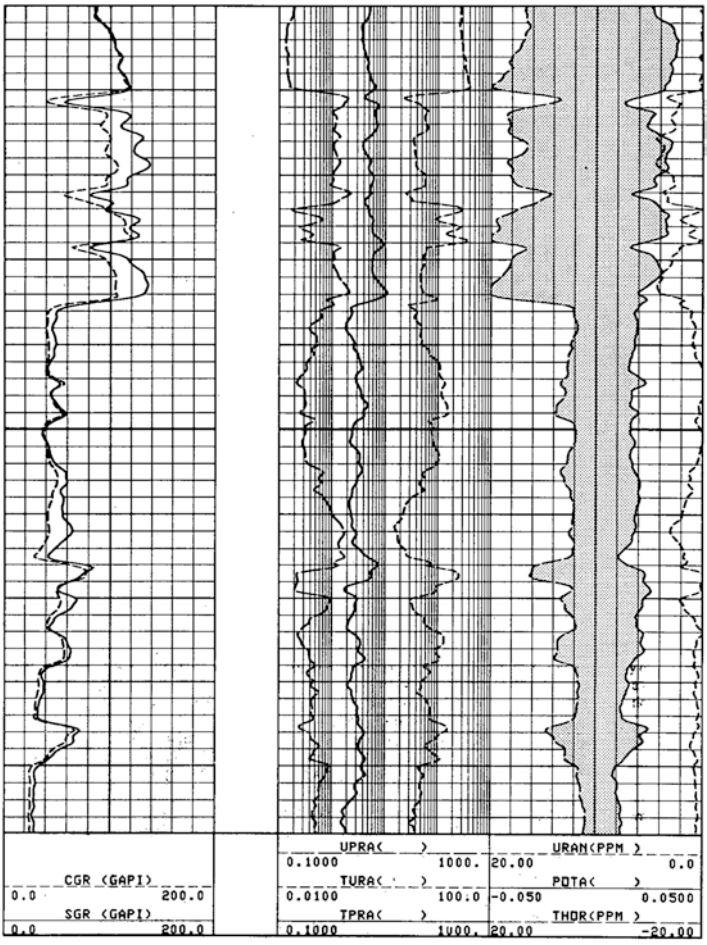

Fig. 11.13 Th, K, and U ratios display. Courtesy Schlumberger

Pulsed Neutron Logging

Pulsed neutron logs provide a means of evaluating a formation after the well has been cased. It is of particular value for:

1. Evaluating old wells, where the original open-hole logs are inadequate or nonexistent.
2. Monitoring reservoir performance over an extended period of time.
3. Monitoring the progress of secondary and tertiary recovery projects.
4. Formation evaluation, as a last resort should the drill-pipe become stuck.

It is one of the most widely used logging methods in cased holes at the present time. Other nuclear measurements that have been developed as extensions of the basic pulsed neutron technology include logs based on the detection of gamma rays resulting from inelastic neutron collisions with nuclei in the formation. These include carbon/oxygen logs and the so-called elemental concentration logs. The same basic tool with some modification can also be used for oxygen activation logging as a flow measuring system. Such applications are covered in Chap. 5.

Principle of Measurement

Many different service company tools are available for use in cased wells. A typical through tubing version will have an OD of 1–11/16″. For use in cased holes without tubing full diameter tools (3–5/8″ OD) are also commonly used. Regardless of the tool used, the principle of measurement remains the same although their operating systems are all slightly different.[2]

A neutron generator is turned on for a very short period of time. As a result, a burst of fast neutrons leaves the tool; and, since neutrons can easily pass through both the steel housing of the tool and the tubing/casing, a cloud of neutrons is formed in the formation. Fast neutrons soon became “thermalized” by collisions with atoms in the formation. The most effective thermalizing agent is the hydrogen present in the pore space in the form of water or hydrocarbon. Once in the thermal state, a neutron is liable to be captured. The capture process depends on the capture cross section of the formation. In general, chlorine dominates the capture process. Since chlorine is present in formation water in the form of salt (NaCl), the ability of the formation to capture thermal neutrons reflects the salt content and hence the water saturation. The capturing of a thermal neutron by a chlorine atom gives rise to a capture gamma ray. Pulsed neutron tools therefore monitor these capture gamma rays. Thus, the common elements of all commercial pulsed neutron tools are (1) a

[2] Historically the first pulsed neutron tool was the Dresser Atlas Nuclear Lifetime Log (NLL) later to become the PDK-100. Schlumberger’s tool was known as the TDT and Halliburton’s as the TMD Descendents of these pioneering tools now go by such trade names as TDT-P, RPM & CRE.

pulsed neutron generator, and (2) gamma ray detectors at different distances from the neutron generator. A generalized neutron tool is shown in Fig. 11.14.

The cloud of neutrons produced by the initial neutron burst from the generator results in a cloud of thermal neutrons in the vicinity of the tool. This cloud dies away due to capture by chlorine atoms or other neutron absorbers in the formation. If there is plenty of chlorine present (i.e., high water saturation), then the cloud of thermal neutrons disappears quite quickly. If, however, hydrocarbons are present (i.e., low water saturation), then the cloud of thermal neutrons decays much more slowly. The rate of decay is measured by monitoring how many capture gamma rays enter the gamma ray counter(s) as a function of time.

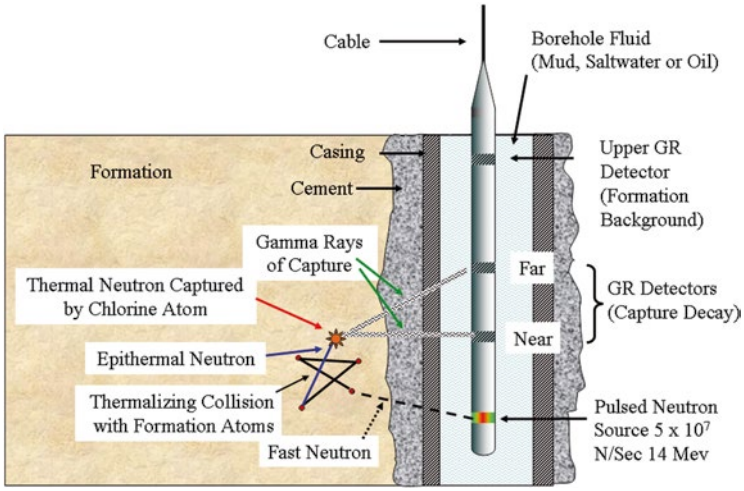

Fig. 11.14 Generalized pulsed neutron tool

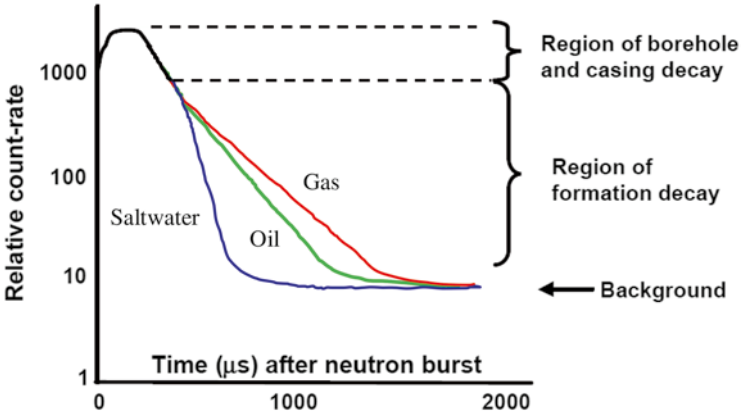

Fig. 11.15 Thermal-neutron decay curves for oil, gas, and water-bearing formations

Figure 11.15 plots the relative counting rate on the *Y*-axis and the time (microseconds) since the initial burst of fast neutrons on the *X*-axis. Note that after a few hundred microseconds a straight-line portion of the decay curve develops. Note also how the water line has a steeper slope than the oil line. Note, too, that at late times the background gamma ray count rate remains substantially constant. The *Y*-axis on Fig. 11.15 is logarithmic, but the time scale (*X*-axis) is linear. Thus, the straight-line portions of the curve represent exponential decays. If N is the number of gamma rays observed at time t and N_o is the number observed at $t=0$, then

$$N = N_o e^{-t/\tau},$$

where τ (Greek letter tau) is the time constant of the decay process. Tau is measured in units of time. It is convenient to quote values of tau in microseconds (1 μs = 10^{-6} s). The capture cross section of the formation, the property of interest, is directly related to tau by the equation

$$\Sigma = 4{,}550 / \tau,$$

where Σ (Greek letter sigma) is the capture cross section measured in capture units (cu). Thus, the essence of measuring Σ is to first find the straight-line portion of the capture gamma ray decay, and then to measure its slope. This is accomplished in different ways by the various commercially available tools.

Log Presentations

On a typical pulsed neutron log, there may be up to nine curves displayed. The curves are illustrated in the Thermal Decay Time (TDT) log presentation of Fig. 11.16

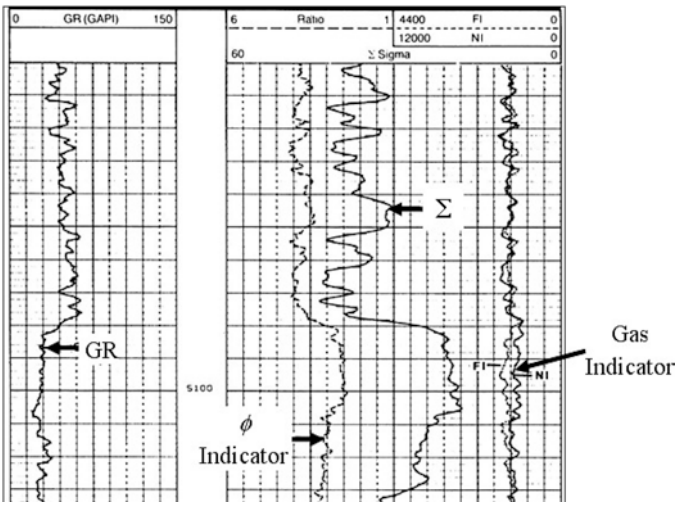

Fig. 11.16 TDT log presentation. Courtesy Schlumberger

Sigma Curve

The Σ curve is the principal pulsed neutron measurement and behaves rather like an open-hole resistivity curve, that is, it deflects to the left (high values of Σ) in wet zones and to the right (low values of Σ) in hydrocarbon-bearing zones or low-porosity formations. Σ values in shales are quite high, tending to mask the effect of hydrocarbons. Thus shaly pay zones can appear to be water-bearing on the first inspection. Figure 11.17 shows a schematic comparison of Σ with resistivity.

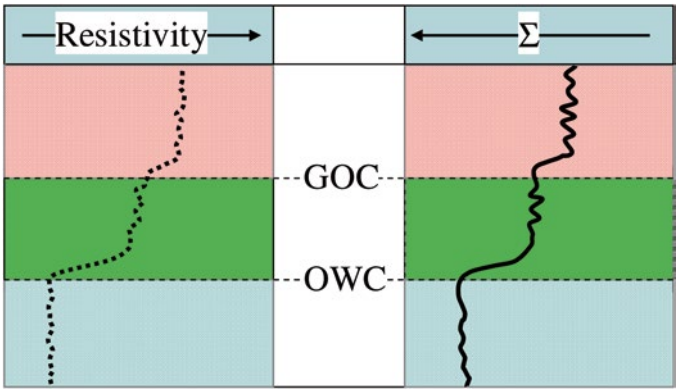

Fig. 11.17 Σ-resistivity comparison

Tau Curve

Tau is just another way of looking at Σ. In fact, τ (the decay-time constant for the thermal-neutron population) is the basic measurement of a pulsed neutron tool. However, all interpretation equations for pulsed neutron logs are linear functions of Σ; and it is much easier to work with Σ rather than with τ. It is recommended that τ be recorded, but left off the log presentation, since its scaled reciprocal, Σ, gives exactly the same information in a form that is easier to work with.

Ratio Curve

The ratio curve is a porosity indicator. It is derived by taking the ratio of the gamma ray counts seen at the near and far detectors respectively. The ratio curve behaves very much like a compensated thermal-neutron (CNL) porosity curve, i.e., it deflects to the right (low ratio) in low porosity, or in the presence of gas. Figure 11.18 shows the ratio curve response to a pocket of gas trapped below a packer behind a tubing nipple. In the absence of any open-hole porosity logs, the ratio can be used in combination with Σ to find formation porosity.

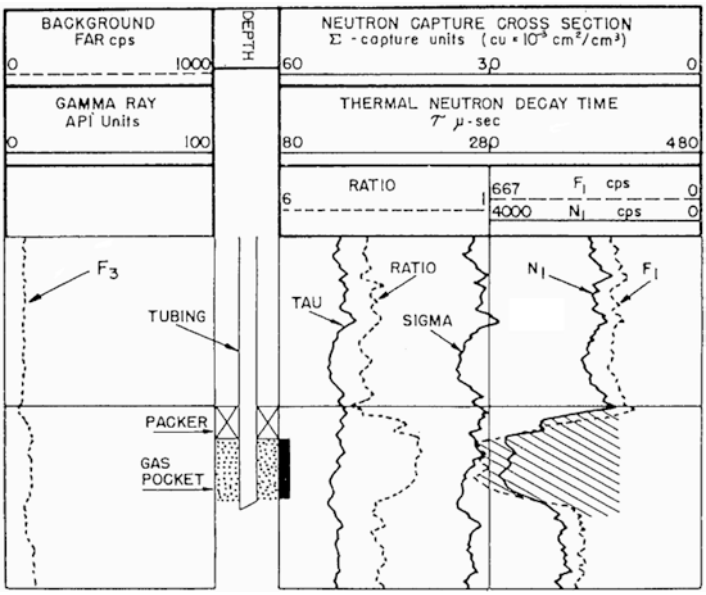

Fig. 11.18 Ratio curve response to gas. Courtesy Schlumberger

Near and Far Count-Rate Display

In Track 3, the near and far count rates are displayed as an overlay. Figure 11.19 illustrates this presentation. When the correct scales are chosen for the near (N_1) and far (F_1) count-rate displays, a useful quick-look log results, with the following properties:

- In 100 % water (section A), $F_1 = N_1$
- In gas (section C), $F_1 > N_1$ (dotted line is left of solid)
- In shales (at the top of the log), $F_1 < N_1$ (dotted line right of solid)

Question # 11.2

Refer to Fig. 11.19

(a) Color code the gas-bearing intervals on the near/far count-rate display using red or pink.
(b) Color code the shale zone at the top of the log green.
(c) Why do you think the oil–water contact is marked where it is (i.e., at 4,535 ft)?
(d) Read the average value of Σ in the water-bearing zone.

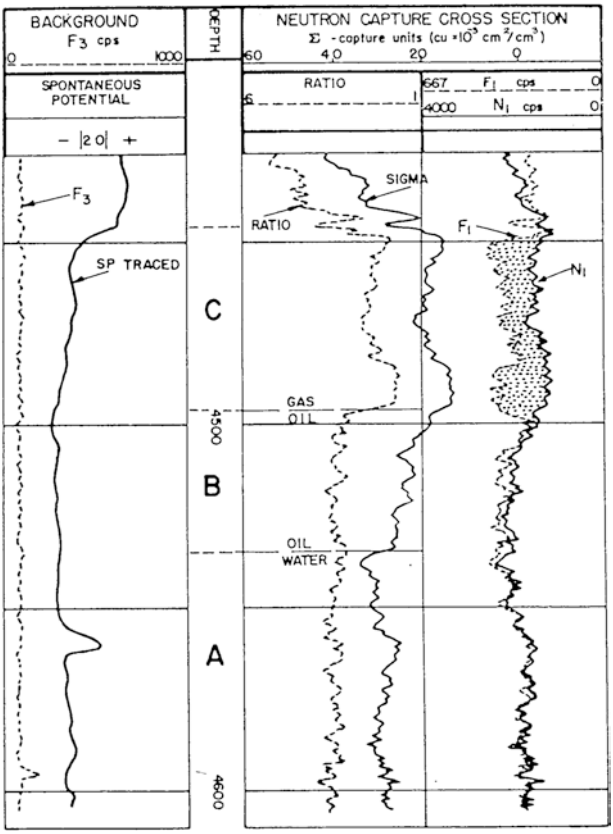

Fig. 11.19 Near/far count-rate display. Courtesy Schlumberger

Background and Quality Curves

The background curve is a very insensitive natural gamma ray curve. There should be little movement on this curve except in "hot" zones which are very radioactive. This curve is sometimes omitted without any great loss.

Summary

The most important curves of the pulsed neutron log are:

Σ	for water saturation
Ratio	for porosity
GR	for shale content
Near/Far display	for gas indications

Capture Cross Sections

The capture cross section of a formation depends on the elements that make up the formation and their relative abundance. Σ values vary over a wide range. The capture cross sections for thermal neutrons are listed in Table 11.1 for a number of elements and in Table 11.2 for various compounds found in rocks.

Table 11.1 Capture cross sections of elements

Element	Σ (cu)
Common elements	
Chlorine	570
Hydrogen	200
Nitrogen	83
Potassium	32
Iron	28
Sodium	14
Sulfur	9.8
Calcium	6.6
Aluminum	5.4
Phosphorus	3.9
Silicon	3.4
Magnesium	1.7
Carbon	0.16
Oxygen	0.01
Rare elements	
Boron	45,000
Cadmium	18,000
Lithium	6,200
Mercury	1,100
Manganese	150

Table 11.2 Capture cross sections of compounds

Compound	Element	Σ (cu)
Basic minerals		
Quartz	SiO_2	4.2
Calcite	$CaCo_3$	7.3
Dolomite	$CaCo_3\ MgCo_3$	4.8
Feldspars		
Albite	$NaAlSi_3o_8$	7.6
Anorthite	$CaAlSi_2O_8$	7.4
Orthoclase	$KAlSi_3o_8$	15
Evaporites		
Anhydrite	$CaSO_4$	13
Gypsum	$CaSO_4 \cdot H_2O$	19
Halite	NaCl	770
Sylvite	KCl	580
Carnallite	$KCl \cdot MgCl_2 \cdot 6H_2O$	370
Borax	$Na_2B_4O_7 \cdot 10H_2O$	9,000
Kernite	$Na_2B_4O_7 \cdot 4H_2O$	10,500
Iron-bearing minerals		
Goethite	FeO(OH)	89
Hematite	Fe_2O_3	104
Magnetite	Fe_3O_4	107
Limonite	$FeO(OH) \cdot 3H_2O$	80
Pyrite	FeS_2	90
Siderite	$FeCO_3$	52
Miscellaneous clays and micas		
Glauconite		22 + 5
Chlorite		25 + 5
Mica/biotite		35 + 10
Pyrolusite	MnO_2	440
Manganite	MnO(OH)	400
Cinnabar	HgS	7,800
Shales		35–55

Basic Interpretation

Clean Formations

Practical interpretation of pulsed neutron logs is conceptually very simple. The total formation capture cross section, Σ, recorded on the log, is just the sum of the products of the volume fractions found in the formation and their respective capture cross sections. Thus, in its simplest form,

$$\Sigma_{\text{Log}} = \Sigma_{\text{matrix}} \cdot (1-\phi) + \Sigma_{\text{fluid}} \cdot \phi$$

Figure 11.20 should clarify the mathematical relationship.

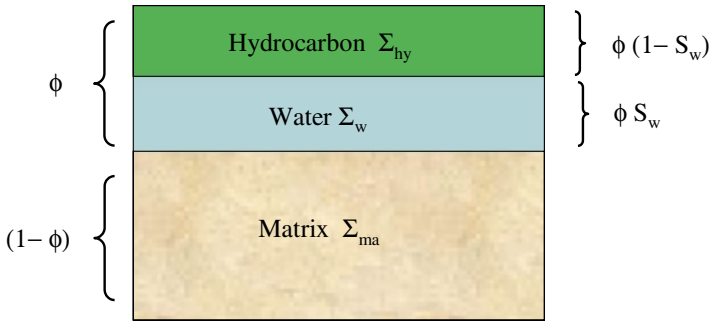

Fig. 11.20 Components of $\boldsymbol{\Sigma}_{Log}$

Of course, the "fluid" may, in fact, be a mixture of oil and water, in which case, the log response is described by:

$$\Sigma_{Log} = \Sigma_{ma}\left(1-\phi\right)+\Sigma_{w}\phi S_{w}+\Sigma_{hy}\phi\left(1-S_{w}\right).$$

By rearrangement of the equation, we have:

$$S_{w}=\frac{\left(\Sigma_{Log}-\Sigma_{ma}\right)-\phi\left(\Sigma_{hy}-\Sigma_{ma}\right)}{\phi\left(\Sigma_{w}-\Sigma_{hy}\right)}$$

Question #11.3
Given: $\Sigma_{Log} = 25.3$ cu.
$\Sigma_{ma} = 10.0$ cu.
$\Sigma_{hy} = 22$ cu.
$\Sigma_{w} = 100$ cu.
$\phi = 30$ %.
Find $S_w =$ _____ .

In the previous example, the values for Σ_{ma}, Σ_{log}, and Σ_w were given. However, in practice, these values may not be known. As a guide, Table 11.3 gives values of Σ for commonly found materials. More exact methods for finding Σ_{ma}, Σ_w, and Σ_{hy} will be covered later in the text.

Log interpretation in clean formations is straightforward. The linear equations can also be thought of graphically. If, for example, a crossplot is made of Σ (on the *Y*-axis) and ϕ, (on the *X*-axis), straight lines represent mixtures of pairs of components.

Table 11.3 Σ values for log interpretation

Σ	Material	Sigma (Cu)
Matrix	Sand	8–10
	Limestone	12
	Dolomite	8
Hydrocarbon	Oil (function of R_s)	22
	Gas (function of γ_g, P, T)	8
Water	Fresh	23
	Seawater	34
	Brine	122

Figure 11.21 shows this method. Note that all water-bearing points fall on the line joining the matrix (porosity = 0, Σ = 10) to the water (porosity = 100, Σ = 100). Likewise, all 100 % oil-bearing points lie on the line joining the matrix to the oil (porosity = 100, Σ = 22). Thus, all points lie inside a solution triangle covered by the matrix, water, and oil points. By simple constructions, lines of constant S_w can be drawn. The dashed lines on Fig. 11.21 join at the point given in Question #11.3, ($\phi = 30$ %, $\Sigma_{Log} = 25.3$).

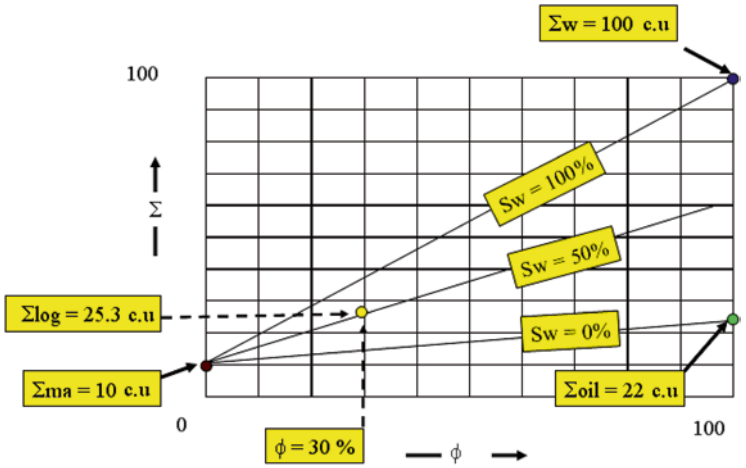

Fig. 11.21 Interpretation in clean formations

How much confidence can be placed in the value of S_w derived as in Fig. 11.21? To a large extent, the accuracy depends on the difference between Σ_{hy} and Σ_w. In fresh formation waters (low Σ_w), the interpretation will be very questionable; but in very salty formation waters (high S_w), it will be reliable. Figure 11.22 illustrates this concept.

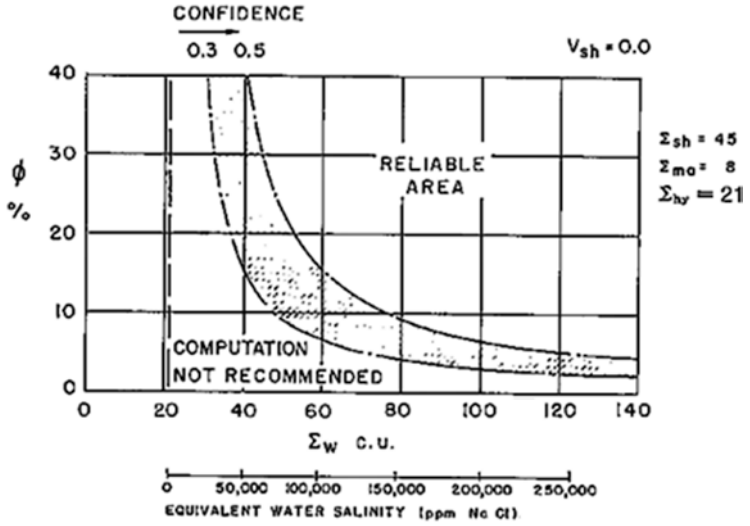

Fig. 11.22 Reliability of S_w Calculation in clean formations. Courtesy Schlumberger

Question #11.4
Color the "reliable" area of Fig. 11.22 with a yellow highlighter
Do the conditions in your district fall in the "reliable" area?

Shaly Formations

The addition of shale to the formation can be handled in the same linear fashion as before. That is:

$$\Sigma_{\text{Log}} = \Sigma_{\text{ma}} \cdot \left(1 - V_{\text{sh}} - \phi\right) + \Sigma_{\text{sh}} V_{\text{sh}} + \Sigma_{\text{w}} \phi S_{\text{w}} + \Sigma_{\text{hy}} \phi \left(1 - S_{\text{w}}\right)$$

which gives:

$$S_{\text{w}} = \frac{\left(\Sigma_{\text{log}} - \Sigma_{\text{ma}}\right) - \phi\left(\Sigma_{\text{hy}} - \Sigma_{\text{ma}}\right) - V_{\text{sh}}\left(\Sigma_{\text{sh}} - \Sigma_{\text{ma}}\right)}{\phi\left(\Sigma_{\text{w}} - \Sigma_{\text{hy}}\right)}$$

Figure 11.23 illustrates the shaly formation. Note that the solution for S_w requires a value for ϕ. In most practical cases, the porosity device used will also be affected by the presence of shale. For example, if a CNL is used as the porosity device, its reading will have to be corrected using:

$$\phi = \phi N - V_{\text{sh}} \cdot \phi N_{\text{sh}},$$

where ϕN is the log reading, V_{sh} is the shale volume % (from GR, etc.), and ϕN_{sh} is the response of the CNL in 100 % shale.

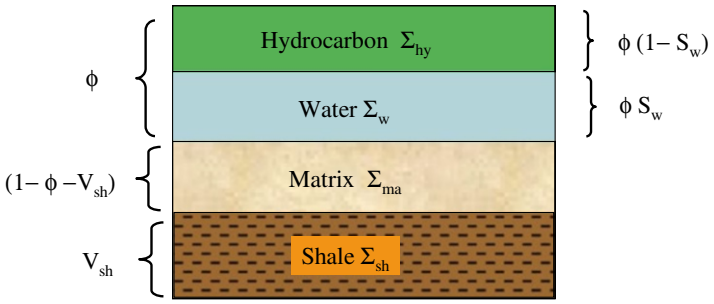

Fig. 11.23 Shaly formation schematic

Question #11.5. Shaly Formation
Given: $\Sigma_{Log} = 30.0$ cu.
$\Sigma_{ma} = 10$ cu.
$\Sigma_{hy} = 22$ cu.
$\Sigma_{w} = 100$ cu.
$\phi N = 37$ %.
$\phi N_{sh} = 35$ %.
$V_{sh} = 20$ %.
$\Sigma_{sh} = 35$ cu.

Find:
(a) $\phi =$ _____ .
(b) $S_w =$ _____ .
(c) $S_w =$ _____ , if you had assumed this was clean instead of a shaly formation.

Note that the equation for Σ_{Log} in shaly formations could be rearranged to read:

$$\Sigma_{Log} = \underbrace{\Sigma_{ma}(1-\phi) + \Sigma_{w}\phi S_{w} + \Sigma_{hy}\phi(1-S_{w}) + V_{sh}(\Sigma_{sh} - \Sigma_{ma})}_{\text{Clean component}} + \underbrace{V_{sh}(\Sigma_{sh} - \Sigma_{ma})}_{\text{Shale component}}$$

Thus, an equally valid method of computing S_w would be to correct Σ_{Log} for shale using the relationship:

$$\Sigma_{cor} = \Sigma_{Log} - V_{sh}(\Sigma_{sh} - \Sigma_{ma}).$$

The value Σ_{cor} can then be used in the normal equation for estimation of water saturation in clean formations. Needless to say, the accuracy of S_w results in shaly formations will be reduced due to uncertainties about the exact values of ϕ, V_{sh}, and Σ_{sh}.

Finding Interpretation Parameters

In order to perform a quantitative interpretation of a pulsed neutron log, certain parameters need to be known. These are:

Σ matrix
Σ water
Σ hydrocarbon (oil and/or gas)
Σ shale

We will now explore various methods of finding these parameters.

Sigma Water

Σ_w is a simple function of the water salinity (ppm NaCl) and temperature (see Fig. 11.24). If the salinity is not known, then a 100 % water-bearing section can give us the required data. Note that if $S_w = 100$, the basic equation reduces to:

$$\Sigma_{Log} = \Sigma_{ma}(1-\phi) + \Sigma_w \phi,$$

which can be rewritten to give:

$$\Sigma_w = \frac{\Sigma_{log} - \Sigma_{ma}(1-\phi)}{\phi}$$

Thus, provided Σ_{ma} and ϕ are known, Σ_w can be back calculated directly. Note that this method is similar to the R_{wa} technique used with open-hole logs. For that reason, the derived value of Σ_w is referred to as Σ_{wa} or *sigma water apparent*. If an extensive water-bearing interval has been logged, a graphical method can provide a "double whammy," both Σ_{ma} and Σ_w from one plot. If pairs of values of Σ and ϕ are plotted on a graph such as the one given in Fig. 11.25, all points at $S_w = 100\,\%$ will fall on a straight line connecting Σ_{ma} (at $\phi = 0\,\%$) and Σ_w (at $\phi = 100\,\%$).

Question #11.6. Σ_w
Given: Formation water salinity = 230,000 ppm NaCl.
Temperature = 200 °F.
Find Σ_w = _____ cu.

Question #11.7. Σ_w
Plot Σ vs. ϕ for the following log readings:

Level	Σ (cu)	ϕ (%)
1	17	28
2	21	32
3	23	26
4	27	28
5	21	13

Level	Σ (cu)	ϕ (%)
6	24	20
7	34	34
8	28	26
9	26	23
10	29	27

Now draw in the $S_w = 100$ % line and find:

(a) $\Sigma_{ma} =$ _____ cu

(b) $\Sigma_w =$ _____ cu

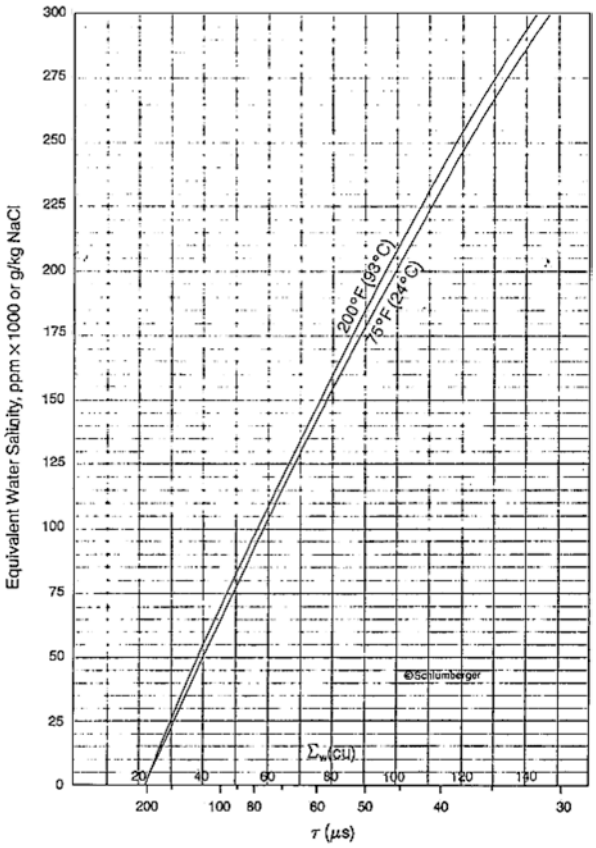

Fig. 11.24 Σ_w as a function of salinity and temperature. Courtesy Schlumberger

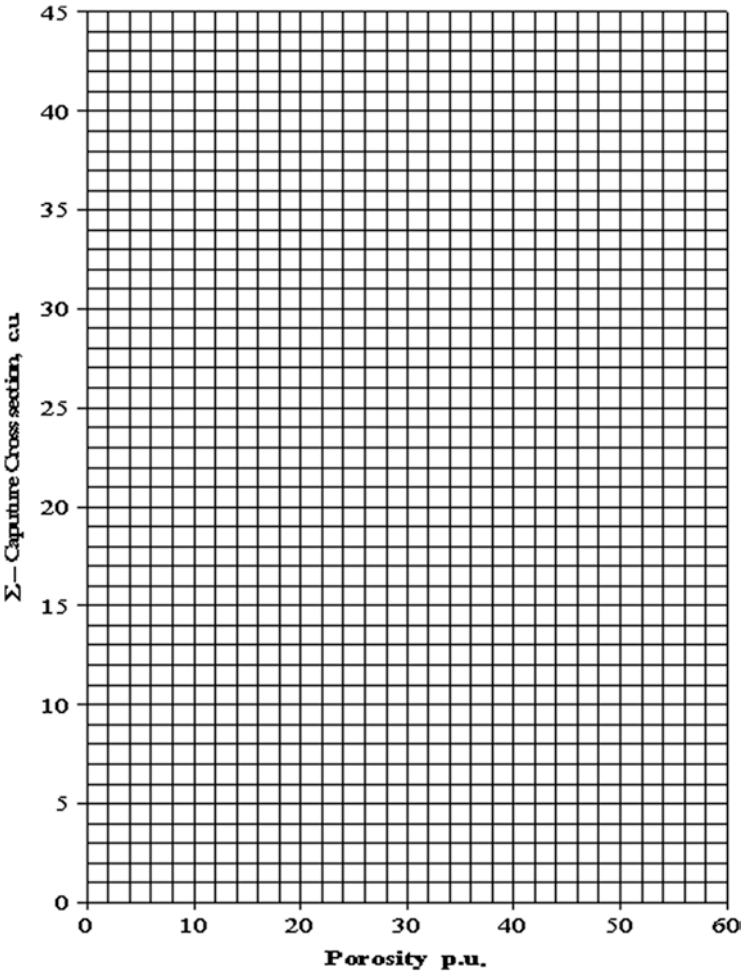

Fig. 11.25 Σ vs. ϕ Crossplot for determination of Σ_{ma} and Σ_{w}.

Sigma Oil

Σ_o is a function of the solution GOR (R_s) of the liquid hydrocarbon in question. Light, gassy oils tend to have lower values of Σ_o. Dead, heavy oils have a minimum Σ_o of about 22 cu. Figure 11.26 shows Σ_o as a function of R_s.

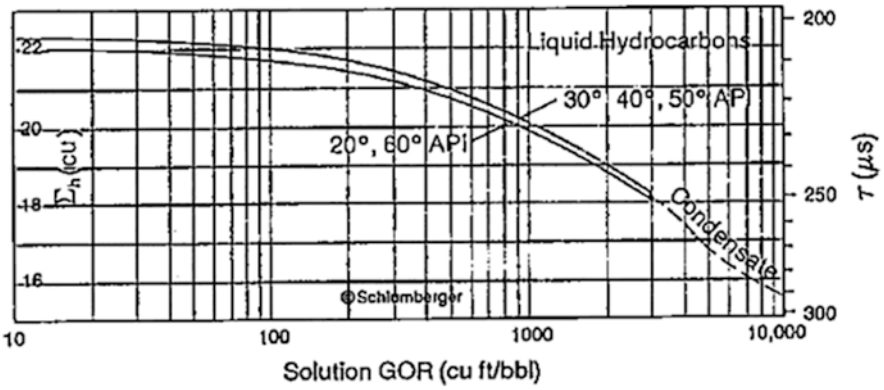

Fig. 11.26 Finding Σ_o. Courtesy Schlumberger

Question #11.8. Σ_o

An oil has a specific gravity of 40° API and an R_s of 400 cu ft/bbl.

Find Σ_o = cu

Sigma Gas

Σ_g is a function of pressure, temperature, and gas gravity. Figures 11.27 and 11.28 allow calculation of Σ_g for a variety of formation conditions. Figure 11.27 finds Σ methane. If the gas in question is methane, then no further work is required. However, if the gas in question is heavier than methane, Fig. 11.28 will convert Σ-CH4 into the appropriate value for Σ gas.

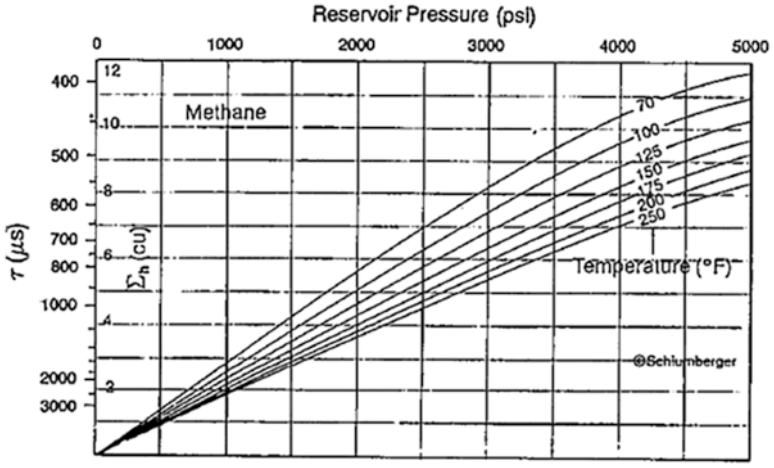

Fig. 11.27 Finding Σ methane. Courtesy Schlumberger

Question #11.9. Σ_g
Given: $p = 3{,}000$ psi.
$T = 150$ °F.
$\gamma_g = 0.65$.
Find $\Sigma_g =$ _____ cu

Sigma Shale

Σ_{sh} may be found by simple inspection of the log. Look for places where:

Gamma reads high
Near/far display indicates shale
Σ_{Log} is relatively high

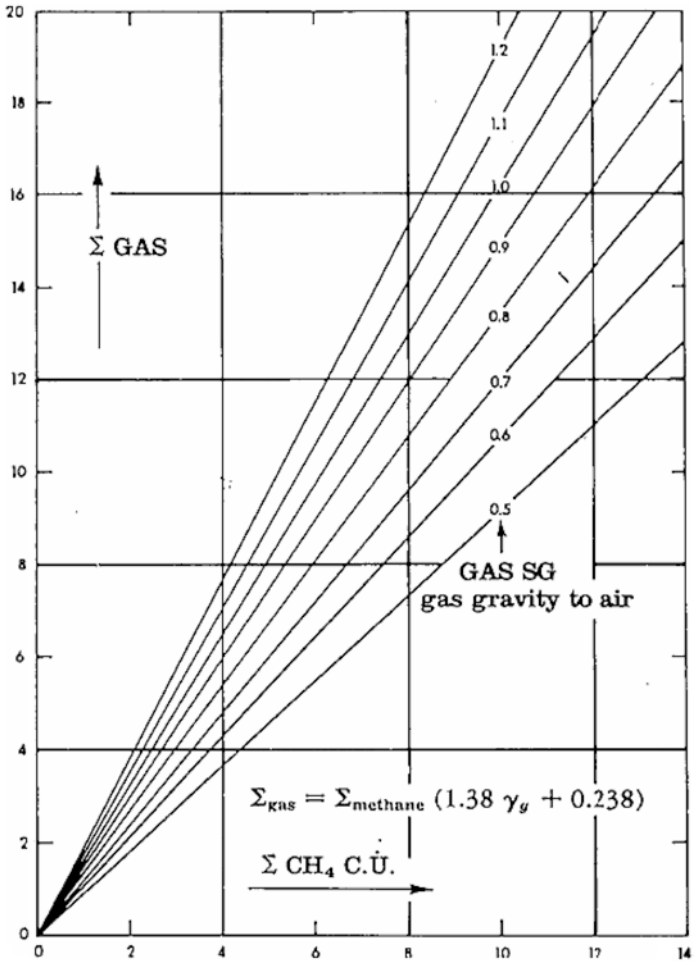

Fig. 11.28 Conversion of Σ methane to Σ gas

Sigma-Ratio Crossplot

If no open-hole logs are available one essential piece of information will be missing, namely, the porosity. Fortunately there is a method for finding porosity from pulsed neutron logs. It requires only the value of sigma and ratio, read directly from the log. These two readings are then cross-plotted to give porosity. A side benefit is that the plot also gives values of Σ_{wa}, the apparent capture cross section of the water. Figure 11.29 gives an example of this type of chart.

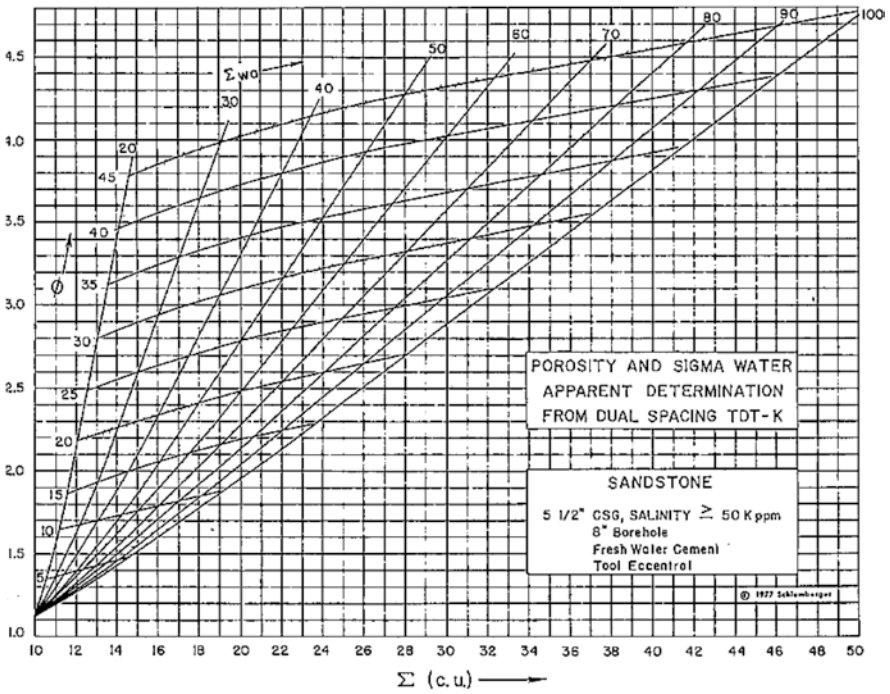

Fig. 11.29 Determination of ϕ and Σ_{wa} from Σ and ratio

It should be noted that many different charts are available form service companies that cover a multitude of different casing sizes and formation water salinities. The particular chart used here for illustrative purposes was built for 5½″ casing and water salinity >50 Kppm NaCl.

Question #11.10. Σ–Ratio Crossplot

A log is run in 5½″ casing with an 8–5/8″ open-hole. The borehole fluid salinity is 80,000 ppm NaCl; $\Sigma_{Log} = 20$ cu and the ratio = 2.8.

(a) Find $\phi =$ _____ %
(b) Find $\Sigma_{wa} =$ _____ cu

Reservoir Monitoring Time-Lapse Technique

Pulsed neutron logs are useful for monitoring the depletion of a reservoir. The *time-lapse* method is used. A base log is run in the well shortly after initial completion but before substantial depletion of the producing horizons. A few days, weeks, or even months of production are required to clean up near well bore effects of the drilling operation, such as mud-filtrate invasion, etc. Once a base log is obtained, the well may be re-logged at time intervals over the life of the field. Typically, a log will be run every six months or once a year, depending on production rate. Successive logs may be overlaid so that changes in saturation can be easily spotted by changes in sigma. A good example of this is given by Fig. 11.30, which shows a base log and three additional logs at roughly 6-month intervals.

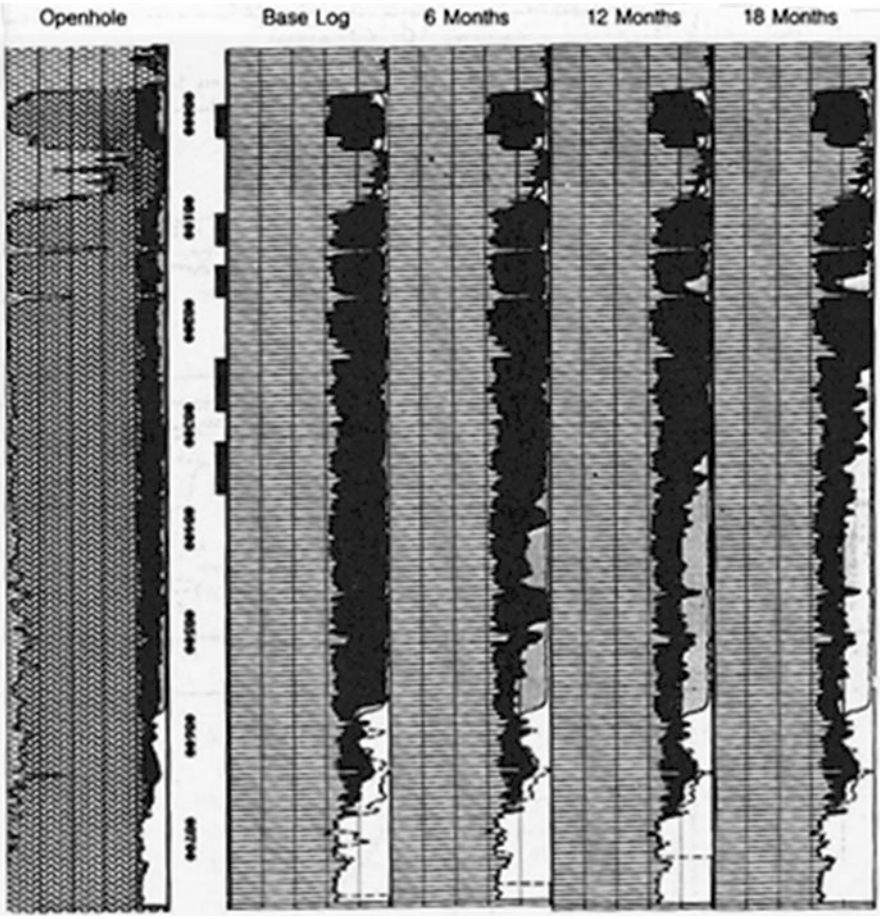

Fig. 11.30 Time-lapse logging

Note the rapid rise of the oil–water contact(s) with passage of time. It is simple to calculate changes in S_w. Consider the state of affairs at time t_1:

$$S_{w1} = \frac{\left(\Sigma_1 - \Sigma_{ma}\right) - \phi\left(\Sigma_{hy} - \Sigma_{ma}\right)}{\phi\left(\Sigma_w - \Sigma_{hy}\right)}$$

and some time later at time t_2:

$$S_{w2} = \frac{\left(\Sigma_2 - \Sigma_{ma}\right) - \phi\left(\Sigma_{hy} - \Sigma_{ma}\right)}{\phi\left(\Sigma_w - \Sigma_{hy}\right)}$$

The change is S_w is, therefore,

$$\Delta S_w = S_{w1} - S_{w2} = \frac{\left(\Sigma_1 - \Sigma_2\right)}{\phi\left(\Sigma_w - \Sigma_{hy}\right)} = \frac{\Delta\Sigma}{\phi\Delta\Sigma_{fluids}}$$

Log-Inject-Log

The log-inject-log technique is used to find residual oil saturations. A base log is run and then the formation is injected with brine and logged again. Finally, the formation is injected with fresh water and logged a third time (see Fig. 11.31).

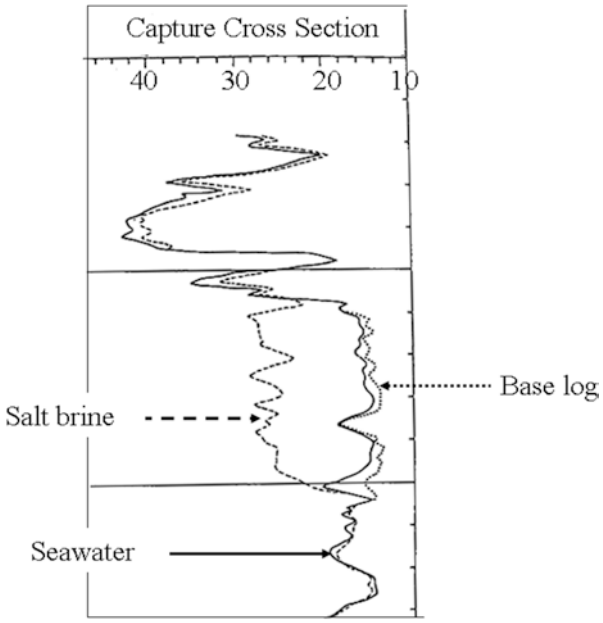

Fig. 11.31 Log-inject-log

Provided the capture cross section of the fresh and brine flushes are known, all the unknown quantities may be normalized out and the residual oil saturation found using:

$$S_o = 1 - \frac{\Sigma_{\text{log brine}} - \Sigma_{\text{log fresh}}}{\phi\left(\Sigma_{\text{brine}} - \Sigma_{\text{fresh}}\right)}$$

Note that it is not necessary to know either Σ_{ma} or Σ_o. The technique has many variations, some of which use specially chlorinated oil that has a high capture cross section.

Departure Curves

Ideally, pulsed neutron logs should be usable for quantitative interpretation without having to make any corrections to the values read from the log. However, in some cases (e.g., when a base log is run with a fresh completion fluid and a subsequent log is run with a salty completion fluid in the borehole, or if the base log is run *without* a liner and a subsequent log *with* a liner), corrections will be required to the raw log measurement of sigma before quantitative interpretation can be made. The required corrections are a function of three variables: casing size, hole size, and salinity of the borehole fluid.

Many sets of departure curves are published by the service companies for their specific tools as functions of open-hole size and casing size. Considerable controversy exists in the literature regarding the need for departure curves. One school of thought holds that the diffusion of neutrons from the borehole to the formation necessitates the use of departure curves. Others maintain that proper tool design and the associated gating systems used to calculate Σ eliminate the need for corrections since they are supposedly free of diffusion effects and the need for departure curves. Some pulsed neutron tool design call for a "dual burst" of neutrons. The decay of the neutron population in the borehole is monitored by a first burst and a second burst is used to monitor the decay in the formation proper.

Essentially pulsed neutron tool design is a delicate balancing act. On the one hand technological advances need to be incorporated in succeeding generations of any given service company's tool. When better gamma ray detectors become available allowing for greater sensitivity, higher count rates, and lower "dead" times then they are incorporated. When additional detectors, above and beyond the basic two conventionally used, then the door is opened for more sophisticated data analysis and better estimates of the true formation Σ, free from the disturbing effect of the borehole Σ. Where the log user is monitoring changes in Σ over time periods longer than tool development cycles sometimes the tool design changes may complicate legitimate log comparisons between today's version of what formation Σ is and what it was 10, 15, or 20 years ago as logged by an older version of the tool which was less technically equipped to unravel the effects of neutron diffusion, etc. As a result multi-detector tools are now emerging on the market (Zett et al. 2012a, b; Bertoli et al. 2013) as well as tools equipped with neutron detectors rather than gamma ray detectors which aim to directly measure the rate of decay of a pulsed package of fast neutrons (Arbuzov et al. 2012).

Depth of Investigation

Another item of interest is the depth of investigation of the pulsed neutron tool. As with most radioactivity measurements, there is no fixed depth of investigation. Rather, a geometric factor describes what percentage of the total signal comes from what radial distance from the borehole wall. Figure 11.32 shows the response of the TDT-K in 5½″ casing with a 1-in. cement sheath. Note that "depth of investigation" is somewhat deeper if salt water has invaded the formation. At all events, the majority of the signal comes from within one foot of the borehole wall.

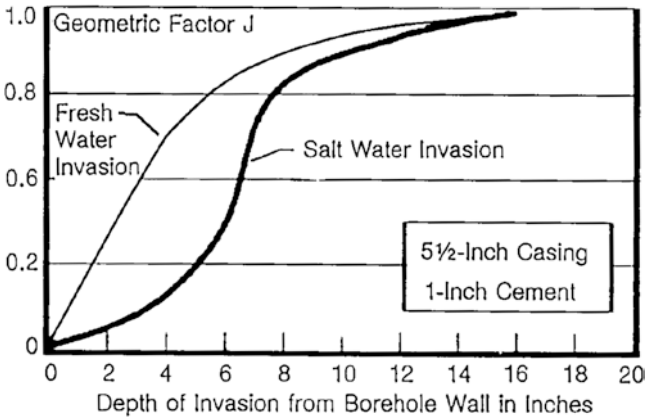

Fig. 11.32 Depth of investigation of typical pulsed neutron measurement

Inelastic Gamma Ray Logging

Neutron logging is continually evolving to reap evermore information about the formations surrounding the tools. Modern versions are used for what is termed elemental spectral analysis. This takes advantage of what are known as inelastic collisions between fast neutrons and the nuclei of the atoms that make up the chemical compounds found in the formation surrounding the cased borehole. When a fast neutron strikes a magnesium nucleus, for example, the nucleus is excited to a higher energy level and then returns to a lower energy level by emitting a gamma ray of characteristic energy. It turns out that the energy of the gamma ray emitted as a result of this inelastic collision can be classified as having come from a magnesium nucleus. Figure 11.33 gives a schematic of a generic neutron logging tool. Note that two annular volumes are depicted surrounding the tool. In the immediate vicinity of the tool is the region where the inelastic interactions take place. Further out radially note that there is a second annular volume of the formation from which gamma rays resulting from capture of thermalized neutrons emanate.

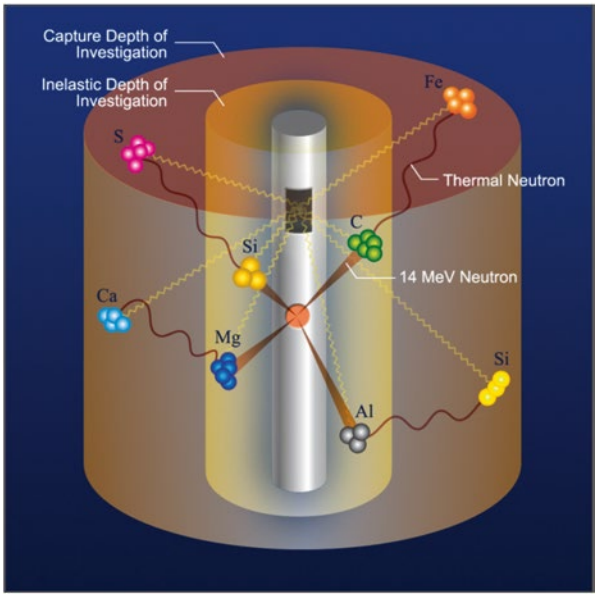

Fig. 11.33 Generic neutron logging tool. Courtesy Baker Hughes

In the figure note that fast neutrons are shown to be inelastically scattered by the nuclei of four elements, Mg, Al, C, and Si. The neutrons thus scattered then are seen to travel outwards to the second annular zone, further from the tool, where, once they are slowed down to thermal energies become captured respectively by atoms of Ca, Si, Fe, and S. The detectors in the tool gather the incoming gamma ray and perform spectroscopic analysis in order to "finger print" the elements present.

Carbon/Oxygen Logging

Initially inelastic neutron scattering was widely used to determine the ratio of carbon to oxygen in the formation surrounding a cased borehole. The underlying principle of the method was the assumption that carbon atoms were to be found in hydrocarbon molecules (e.g., gas and/or oil, C_nH_{2n+2}) and oxygen atoms found in water (H_2O). Thus, depending on the porosity, the C/O ratio would be an indicator of formation water saturation, S_w.

Figure 11.34 shows a typical "fan chart" relating the measured C/O ratio to $S_{w.}$ Note that there are two "fans" with one labeled "Sandstone" and the other "Limestone". The reason for this is the ambiguity of any given value for the C/O ratio. If the formation matrix is free of any carbon then, for example, a C/O ratio of 0.14 coupled with a formation porosity of 27.5 % would indicate a water saturation of zero. However the same log reading and porosity would indicate 100 % water if the matrix were limestone. This characteristic of C/O logs need not be fatal provided the logging is performed where the matrix elemental composition is known and/or the device is used to solely to monitor oil/water or gas/oil contact changes over time by performing repeat logs over the productive life of the reservoir.

C/O Logging for TOC

With the increased interest in characterizing the organic richness of shale gas reservoirs the C/O log has had a revival in that it affords and way to estimate the value of the all important TOC number. If the oxygen content of the formation is known then the carbon content can be calculated using:

$$C = C/O \times O$$

In turn the oxygen content of the formation can be calculated using:

$$O_{\text{formation}} = O_{\text{matrix}} + O_{\text{fluid}}$$

O_{matrix} will depend on the matrix material but surprisingly it does not vary very much as is shown in Table 11.4. For most commonly occurring organic rich shales the oxygen content lies in the range of 48–53 %.

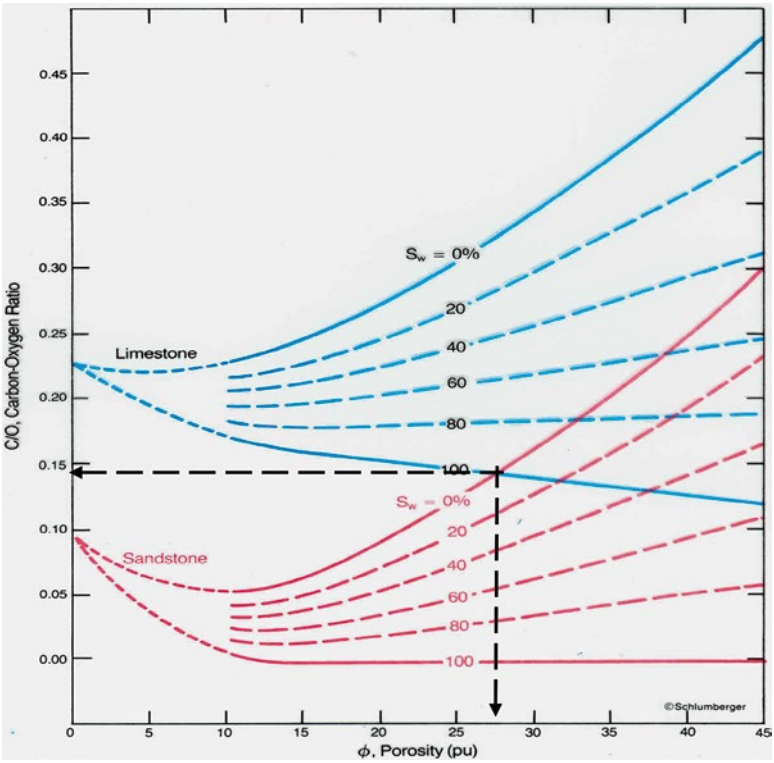

Fig. 11.34 Ambiguous C/O interpretation. Courtesy Schlumberger

O_{fluid} is based on an assumption that the fluid is water in which case it is equal to 89 %. Based on these assumptions, the formation oxygen content be calculated as follows:

$$O_{\text{formation}} = 0.89 \times \phi \times \rho_{\text{fluid}} + 0.53 \times (1 - \phi) \times \rho_{\text{matrix}}$$

For a C/O ratio of 0.1 even as ρ_{matrix} varies from 2.4 g/cc to 3 g/cc the calculated total carbon decreases by less than 0.1 wt% so the choice of ρ_{matrix} is very forgiving and one is justified in leaving it at 2.65 for a first approximation.

The oxygen content organic material (gas, oil, kerogen, etc.) is zero. Thus the formation oxygen content will also depend on the water saturation within the pore space available.

Table 11.4 Oxygen content of matrix materials (After Herron)

Mineral	Wt % O
Siderite	41
Orthoclase	46
Anorthite	47
Calcite	48
Albite	49
Illite	51
Dolomite	52
Quartz	53
Kaolinite	56
Gypsum	56
Montmorillonite	59

Total Carbon content of the formation is thus derived from the C/O ratio read from the log and an estimate of the formation oxygen content. However the carbon present in the formation may be in the form of organic carbon but could also be present in the form of carbonates such as calcite and dolomite. An independent measurement is thus required to "back out" the effect of any carbonate present. For this the same wireline inelastic gamma ray tool can be used to measure the calcium content of the formation and from there calculate the TOC as:

$$\text{TOC} = C_{\text{Total}} - C_{\text{Carbonates}}$$

An example calculation:

Porosity is 10 %, therefore,

$$O_{\text{formation}} = 0.89 \times 0.1 \times 1 + 0.53 \times 0.9 \times 2.65 = 1.35$$

And if the C/O ratio is 0.1 then,

$$C_{\text{total}} = 0.1 \times 1.35 = 0.135$$

If the carbon content of the formation due to carbonates is 10 % then the TOC would be given by:

$$\text{TOC} = 0.135 - 0.1 = 0.035 \text{ or } 3.5\%$$

Cased-Hole Wireline Formation Tester

Wireline formation testers are routinely used in open hole before casing is set in order to evaluate the formation pressure, permeability, and fluid content. The technology developed for such testing is also applicable to cased holes with some modifications. Essentially a standard tool is adapted to include the means to make a hole through the casing and cement and a way to seal such a hole when the test is complete. One embodiment of such a testing tool is shown in Fig. 11.35.

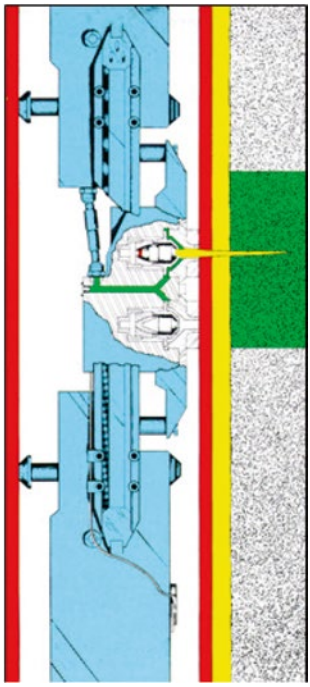

Fig. 11.35 Cased-hole wireline formation tester

The hole making part can be accomplished by either a motorized drill or by an explosive shaped charge. Once communication is established between the tool's plumbing and the formation beyond the casing and cement the actual testing is analogous to that performed in an open-hole test. Sealing of the hole is accomplished by injection of an appropriate epoxy sealer or similar substance. Application for these kinds of tools can be found in work-over situations where there is a lack of data in the well files and there is uncertainty regarding the current formation fluid content and pressure.

Appendix 1: Interpretation of Pulsed Neutron Logs Using the Dual-Water Method

The dual-water method of interpreting pulsed neutron logs is based on the assumption that shales are composed of dry clay, crystalline minerals to whose surface is bound a layer of water. This water is called *bound water*. A further assumption is that the properties of bound water (e.g., R_w, Σ_w) may be different from those of *free water* that exists in the effective, interconnected pore space. In particular, the theory of dual-water interpretation proposes that bound water is less saline than free water in most cases. Correct interpretation, therefore, calls for a means to find the amount of (1) dry clay and (2) bound water. The concept of *total porosity* ϕ_T, that is, the free fluids, ϕ_e, and the bound water, is an important part of the theory. Figure 11.36 illustrates the concepts by mapping bulk volume fractions of a shaly formation.

The following relationships pertain:

$$\phi_e = \phi_T - V_{wb}.$$

$$S_{wT} = \left(V_{wf} + V_{wb}\right) / \phi_T.$$

$$S_{we} = V_{wf} / \phi_e.$$

$$V_{sh} = V_{wb} + V_{dc}.$$

Essentially, there are five unknown quantities: $V_{ma}, V_{dc}, V_{wb}, V_{wf}$, and V_{hy}. The logs available are Σ, ratio, and GR. The identity:

$$V_{ma} + V_{dc} + V_{wb} + V_{wf} + V_{hy} = 1$$

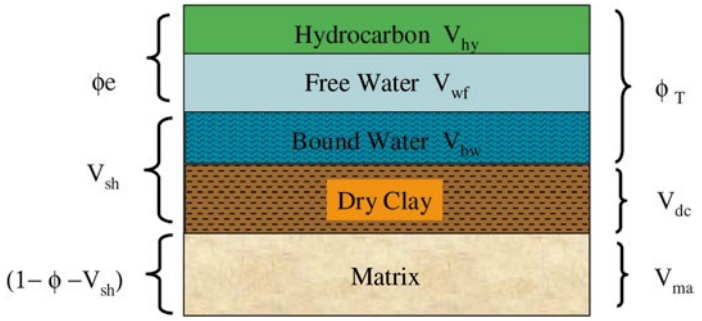

Fig. 11.36 Dual-water shaly formation

adds one more for a total of four measurements. Therefore, one unknown must be eliminated before a solution can be found. The normal way of doing this is to make an assumption about V_{wb} as a function of V_{dc}. That is, to assume that a unit volume of dry clay always has associated with it the same amount of bound water. In fact, in "pure shale," it would be quite common to find a "total porosity" of 30 or 40 % (as reflected by neutron log readings in shales). In this case, the amount of bound water associated with a dry clay can be back calculated.

For example, if a 100 % shale has a total porosity of 35 %, it follows that:

$$V_{wb} = 35\% \text{ and } V_{dc} = 65\%$$

and hence that:

$$V_{wb} = \alpha \cdot V_{dc},$$

where α is some constant which, in this example, is numerically equal to $35/65 = 0.538$. Having reduced the unknowns to four (V_{ma}, V_{dc}, V_{wf}, and V_{hy}), since V_{wb} can now be assumed equal to $\alpha \cdot V_{dc}$, the solution to the dual-water problem becomes straightforward.

The following steps are required:

1. Find all necessary parameters Σ_{ma}, Σ_{dc}, Σ_{wf}, Σ_{hy}, GR_{ma}, GR_{dc}.
2. Find ϕ_T and V_{dc}.
3. Solve for ϕ_e and S_{we}.

Finding Parameters

Crossplot techniques are particularly useful for finding the required parameters. The log data points should be divided into two groups: The 100 % shales and the clean-formation intervals. In clean formations, a plot of Σ vs. ϕ will define Σ_{ma} and Σ_{wf}, provided there is sufficient variation in porosity and enough points at 100 % water saturation. Figure 11.37 shows the procedure schematically.

A similar plot for finding Σ_{dc} and Σ_{wb} is shown in Fig. 11.38 (all points must come from the shale sections). Note that, on both plots, ϕ_T, derived from the Σ vs. ratio crossplot, is used. This entails an assumption that porosity measured in this way is, in fact, equal to total porosity.

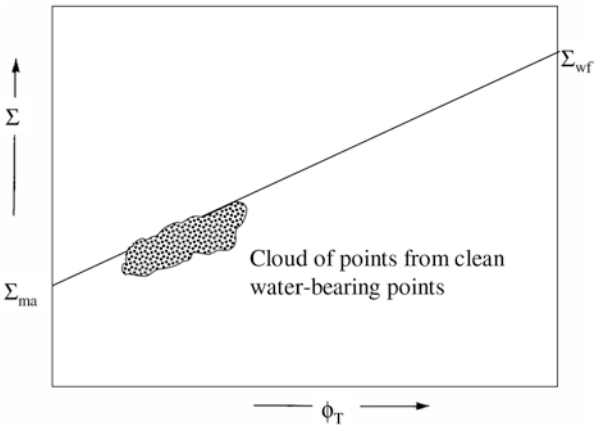

Fig. 11.37 Finding Σ_{ma} and Σ_{wf}.

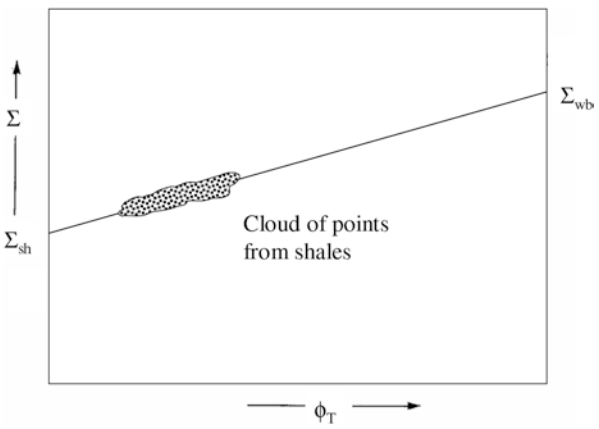

Fig. 11.38 Finding Σ_{dc} and Σ_{sb}

Σ_{hy} can be found by conventional means. Thus, only the gamma ray response to dry clay and response to the matrix remain to be found. It is assumed that neither formation water nor hydrocarbon contribute to the gamma ray response, so it can be written

$$\mathrm{GR} = \left(1-\phi_{\mathrm{T}}\right)\ \mathrm{GR}_{\mathrm{ma}} + V_{\mathrm{dc}}\,\mathrm{GR}_{\mathrm{dc}}.$$

From which it follows that, in shales,

$$\mathrm{GR}_{\mathrm{dc}} = \mathrm{GR}/\left(1-\phi_{\mathrm{T}}\right),$$

and, in clean intervals,

$$\mathrm{GR}_{\mathrm{ma}} = \mathrm{GR}/\left(1-\phi_{\mathrm{T}}\right).$$

For example, in a shale, GR = 110 and $\phi_T = 33$ %; but, in a clean section, GR = 25 and $\phi_T = 25$ %, so it follows that:

$GR_{dc} = 110/(1-0.33) = 149.25$, and

$GR_{ma} = 25/(1-0.25) = 33.3$.

Finding ϕ_T and V_{dc}

As already stated, ϕ_T is found from the Σ vs. ratio crossplot. V_{dc} can be found from the *GR* using:

$$V_{dc} = \frac{GR - GR_{ma}\left(1-\phi_T\right)}{GR_{dc} - GR_{ma}}$$

Solving for ϕ_e and S_{we}

Once V_{dc} and ϕ_T are established, the following relationships hold:

$\phi_e = \phi_T - V_{wb}$ (which also $= V_{hy} + V_{wf}$),

$V_{ma} = 1 - \phi_T - V_{dc}$, and $V_{wb} = \alpha V_{dc}$,

where α has been established in the shales as $\phi_{Tsh}/(1-\phi_{Tsh})$.

The response of the pulsed neutron log itself can be written as:

$$\Sigma = \Sigma_{ma} V_{ma} + \Sigma_{dc} V_{dc} + \Sigma_{wb} \alpha V_{dc} + \Sigma_{wf} V_{wf} + \Sigma_{hy} V_{hy},$$

hence:

$$\Sigma_{hy} V_{hy} + \Sigma_{wf} V_{wf} = \Sigma - \Sigma_{ma} V_{ma} - V_{dc}\left(\Sigma_{dc} + \alpha \Sigma_{wb}\right).$$

The right side of the equation can be evaluated since all the parameters and variables have now been defined. If this quantity is, in fact, Σ*, then

$$V_{wf} = \frac{\Sigma^* - \phi_e \Sigma_{hy}}{\Sigma_{wf} - \Sigma_{hy}}$$

By definition,

$$S_{we} = V_{wf} / \phi_e.$$

Appendix 2: Radioactive Elements, Minerals, and Rocks

Table 11.5 Natural gamma ray emitters

Nuclide		Mode of disintegration	Half-life
Uranium series			
UI	$_{92}U^{238}$	α	4.51×10^4 years
UX_1	$_{90}Th^{234}$	β	24.1 days
UX_2	$_{91}Pa^{234m}$	β, IT	1.18 min
UZ	$_{91}Pa^{234}$	β	6.66 h
UII	$_{92}U^{234}$	α	2.48×10^4 years
Io	$_{90}Th^{230}$	α	8.0×10^4 years
Ra	$_{88}Ra^{226}$	α	1620 years
Rn	$_{86}Em^{222}$	α	3.82 days
RaA	$_{84}Po^{218}$	α, β	3.05 min
RaA′	$_{85}At^{218}$	α, β	2 s
RaA″	$_{86}Em^{218}$	α	1.3 s
RaB	$_{82}Pb^{214}$	β	26.8 min
RaC	$_{83}Bi^{214}$	α, β	19.7 min
RaC′	$_{84}Po^{214}$	α	1.6×10^{-4} s
RaC″	$_{81}TI^{210}$	β	1.32 min
RaD	$_{82}Pb^{210}$	β	19.4 years
RaE	$_{83}Bi^{210}$	α, β	5.01 days
RaF	$_{84}Po^{210}$	α	138.4 days
RaE′	$_{81}TI^{206}$	β	4.2 min
RaG	$_{82}Pb^{206}$		Stable
Thorium series			
Th	$_{90}Th^{232}$	α	1.42×10^{10} yr
$MsTh_1$	$_{88}Ra^{228}$	β	6.7 years
$MsTh_2$	$_{89}Ac^{228}$	β	6.13 h
RdTh	$_{90}Th^{228}$	α	1.91 years
ThX	$_{88}Ra^{224}$	α	3.64 days
Tn	$_{86}Em^{220}$	α	51.5 s
ThA	$_{84}Po^{216}$	α	0.16 s
ThB	$_{82}Pb^{212}$	β	10.6 h
ThC	$_{83}Bi^{212}$	α, β	60.5 min
ThC′	$_{84}Po^{212}$	α	0.30 μs
ThC′	$_{81}T^{208}$	β	3.10 min
ThD	$_{82}Pb^{208}$		Stable

Table 11.6 Gamma ray lines[a] in the spectra of the important naturally occurring radionuclides

Nuclide	Gamma ray energy (MeV)	Number of photons per disintegration in equilibrium mixture
Bi^{214}(Rac)	0.609	0.47
	0.769	0.05
	1.120	0.17
	1.238	0.06
	1.379	0.05
	1.764	0.16
	2.204	0.05
$T4^{208}$(ThC′)	0.511	0.11
	0.533	0.28
	2.614	0.35
K^{40}	1.46	0.11

[a]With intensities greater than 0.05 photons per disintegration and energies greater than 100 kev

Table 11.7 Thorium-bearing minerals

Name	Composition	ThO_2 content %
Thorium minerals		
Cheralite	$(Th, Ca, Ce)(PO_4SiO_4)$	30, variable
Huttonite	$ThSiO_4$	81.5 (ideal)
Pilbarite	$ThO_2 \cdot UO_3 \cdot PbO \cdot 2SiO_2 \cdot 4H_2O$	31, variable
Thorianite	ThO_2	Isomorphous series to UO_2
Thorite[a]	$ThSiO_4$	25 to 63-81.5 (ideal)
Thorogummite[a]	$Th(SiO_4)_{1-x}(OH)_{4-x}$; $x < 0.25$	24–58 or more
Thorium-bearing minerals		
Allanite	$(Ca, Ce, Th)_2(Al, Fe, Mg)_3Si_3O_{12}(OH)$	0 to about 3
Bastnaesite	$(Ce, La)Co_3F$	Less than 1
Betafite	About $(U, Ca)(Nb, Ta, Ti)_30_9 \cdot nH_20$	0 to about 1
Brannerite	About $(U, Ca, Fe, Th, Y)_3Ti_5O_{16}$	0–12
Euxenite	$(Y, Ca, Ce, U, Th)(Nb, Ta, Ti)_2O_5$	0 to about 5
Eschynite	$(Ce, Ca, Fe, Th)(Ti, Nb)_2O_6$	0–17
Fergusonite	$(Y, Er, Ce, U, Th)(Nb, Ta, Ti)O_4$	0 to about 5
Monazite[b]	$(Ce, Y, La, Th)PO_4$	0 to about 30; usually 4–12
Samarskite	$(Y, Er, Ce, U, Fe, Th)(Nb, Ta)_2O_6$	0 to about 4
Thucholite	Hydrocarbon mixture containing U, Th, rare earth elements	
Uraninite	UO_2 (ideally) with Ce, Y, Pb, Th, etc.	0–14
Yttrocrasite	About $(Y, Th, U, Ca)_2(Ti, Fe, W)_4O_{11}$	7–9
Zircon	$ZrSiO_4$	Usually less than 1

Source: After Frondel, C., 1956, in Page, L. R., Stocking, H. E., and Smith, H. D., Jr., U.S. Geol. Survey Prof. Papers no. 300

[a]Potential thorium ore minerals

[b]Most important commercial ore of thorium. Deposits are found in Brazil, India, USSR, Scandinavia, South Africa, and the USA

Table 11.8 Uranium minerals

Autunite	$Ca(UO_2)_2(PO_4)_2$ 10-12H_2O
Tyuyamunite	$Ca(UO_2)_2(VO_4)_2$ 5-8H_2O
Carnotite	$K_2(UO_2)_2(UO_4)_2$ 1-3H_2O
Baltwoodite	U-silicate high in K
Weeksite	U-silicate high in Ca

Table 11.9 Potassium, Uranium, and Thorium distribution in rocks and minerals

	K (%)	U (ppm)	Th (ppm)
Accessory minerals			
Allanite		30–700	500–5,000
Apatite		5–150	20–150
Epidote		20–50	50–500
Monazite		500–3,000	2.5×10^4–20×10^4
Sphene		100–700	100–600
Xenotime		500-3, 4×10^4	Low
Zircon		300–3,000	100–2,500
Andesite (av.)	1.7	0.8	1.9
A., Oregon	2.9	2.0	2.0
Basalt			
Alkali basalt	0.61	0.99	4.6
Plateau basalt	0.61	0.53	1.96
Alkali olivine basalt	<1.4	<1.4	3.9
Tholeiites (orogene)	<0.6	<0.25	<0.05
(non orogene)	<1.3	<0.50	<2.0
Basalt in Oregon	1.7	1.7	6.8
Carbonates			
Range (average)	0.0–2.0 (0.3)	0.1–9.0 (2.2)	0.1–7.0(1.7)
Calcite, chalk, Limestone, olomite (all pure)	<0.1	<1.0	<0.5
Dolomite, West Texas (clean)	0.1-0.3	1.5-10	<2.0
Limestone (clean)			
Florida	<0.4	2.0	1.5
Cretaceous trend, Texas	<0.3	1.5-15	<2.0
Hunton lime, Okla.	<0.2	<1.0	<1.5
West Texas	<0.3	<1.5	<1.5
Clay minerals			
Bauxite		3–30	10–130
Glauconite	5.08–5.30		
Bentonite	<0.5	1–20	6–50
Montmorillonite	0.16	2–5	14–24
Kaolinite	0.42	1.5–3	6–19
Illite	4.5	1.5	
Mica			

(continued)

Table 11.9 (continued)

	K (%)	U (ppm)	Th (ppm)
Biotite	6.7–8.3		<0.01
Muscovite	7.9–9.8		<0.01
Diabase, Va.	<1.0	<1.0	2.4
Diorite, quartzodiorite	1.1	2.0	8.5
Dunite, Wa.	<0.02	<0.01	<0.01
Feldspars			
Plagioclase	0.54		<0.01
Orthoclase	11.8–14.0		<0.01
Microcline	10.9		<0.01
Gabbro (mafic igneous)	0.46–0.58	0.84–0.9	2.7–3.85
Granite (silic igneous)			
Rhode Island	2.7–4.26	3.6–4.7	19-20
New Hampshire	4.5–5	4.2	25–52
Precambrian (Okla.)	3.5–5	12–16	50–62
Minnesota, (Col. Tex.)	2–6	3.2–4.6	14–27
Grandodiorite	2–2.5	2.6	9.3–11
Colorado, Idaho	5.5	2–2.5	11.0–12.1
Oil shales, Colorado	<4.0	up to 500	1–30
Periodite	0.2	0.01	0.05
Phosphates		100–350	1–5
Rhyolite	4.2	5	
Sandstones, range (av.)	0.7–3.8 (1.1)	0.2–0.6 (0.5)	0.7–2.0 (1.7)
Silica, quartz, quartzite, (pure)	<0.15	<0.4	<0.2
Beach Sands, Gulf Coast	<1.2	0.84	2.8
Atlantic Coast (Fla., N.C.)	0.37	3.97	11.27
Atlantic Coast (N.J., Mass.)	0.3	0.8	2.07
Shales			
“Common” shales [range (av.)]	1.6–4.2 (2.7)	1.5–5.5 (3.7)	8–18 (12.0)
Shales (200 samples)	2.0	6.0	12.0
Schist (biotite)		2.4–4.7	13–25
Syenite	2.7	2,500	1,300
Tuff (feldspatic)	2.04	5.96	1.56

Table 11.10 Geological significance of natural gamma ratios

Ratios	Remarks
Thorium/ Uranium (Th/U)	In *sedimentary* rocks, Th/U varies with depositional environment Th/U
	>7: continental, oxidizing environment, weathered soils, etc.
	<7: marine deposits, gray and green shales, graywackes
	<2: marine black shales, phosphates
	In *igneous* rocks, high Th/U indicative of oxidizing conditions by magma
	Before crystallization and/or extensive leaching during
	Postcrystallization history
	Source rock potential estimates of argillaceous sediments (shales)
	Major geologic unconformities
	Distance to ancient shore lines or location of rapid uplift during time of deposition
	Stratigraphic correlations, transgression vs. regression, oxidation vs. reduction regimes, etc.
Uranium/ Potassium (U/K)	Source rock potential of argillaceous sediments
	Stratigraphic correlations
	Unconformities, diagenetic changes in argillaceous sediments, carbonates, etc.
	Frequent correlation with vugs and natural fracture systems in subsurface formations, including localized correlation with hydrocarbon shows on drilling mud logs and core samples both in clastic and carbonate reservoirs
Thorium/ Potassium (Th/K)	Recognition of rock types of different facies
	Paleographic and paleoclimatic interpretation of facies characteristics
	Depositional environments, distance from ancient shore lines, etc.
	Diagenetic changes of argillaceous sediments
	Clay typing: Th/K increases from glauconite ⇒ muscovite ⇒ illite ⇒ mixed-layer clays ⇒ kaolinite ⇒ chlorite ⇒ bauxite
	Correlation with crystallinity of illite, average reflectance power, paramagnetic electronic resonance

Bibliography

Al-Nasser MN, Ma M, Al-Mushrafi N, Al-Muthana AS, Riley S, Geevarghese AI. Quantifying gas saturation with pulsed neutron logging—an innovative approach. SPE 166025-MS. 2013.

Antkiw S. Depth of investigation of the dual-spacing thermal neutron decay time logging tool. In: SPWLA Trans. 17th Logging Symposium, Denver, Colo. 1976.

Arbuzov AA, Alekhin AP, Bochkarev VV, Minakhmetova RN, Chukhutin DV, Zakirov AN. Memory pulsed neutron-neutron logging. In: SPE Russian oil and gas exploration and production technical conferences and exhibition held in Moscow, Russia 16-18 October, SPE 162074. 2012.

Bertoli S, Borghi M, Galli G, Oprescu A, Riley S. Field trials of a new array pulsed neutron formation gas measurement in complex completions. Presented at the 11th Offshore Mediterranean Conference and Exhibition in Ravenna, Italy, March 20-22. 2013.

Blackburn JS, Brimage RC. Estimation of formation pressures in clean gas sands from the dual-spacing TDT log. In: SPWLA Trans. 19th Logging Symposium, EI Paso, Tex. 1978.

Clavier C, Hoyle W, Meunier D. Quantitative interpretation of thermal neutron decay time logs: part I. Fundamentals and techniques, part II. Interpretation examples, interpretation accuracy, and time-lapse technique. J Petrol Tech. 1971;23:743–63.

Departure curves for the thermal decay time log. Schlumberger, Publication C-11989; 1976.

Dewan JT, Johnstone CW, Jacobson LA, Wall WB, Alger RP. Thermal neutron decay time logging using dual detection. In: SPWLA Trans. 14th Logging Symposium, Lafayette, LA, May 1973.

Fertl WH, Frost Jr E. Experiences with natural gamma ray spectral logging in North America. Paper SPE 11145 presented at the SPE 57rd annual technical conference and exhibition, New Orleans, Sept. 25-29, 1982.

Fertl WH, Stapp WL, Vaello DB, Vercellino WC. Spectral gamma ray logging in the Texas Austin Chalk trend. J Petrol Tech. 1980; Presented at the SPE 53rd annual technical conference and exhibition, Houston, Oct. 1–4, 1978.

Frondel C. L. R. Page, H. E. Stocking, and H. B. Smith, U.S. Geol. Survey Prof. Papers No. 300; 1956.

Gadeken LL, Arnold DM, Smith Jr HD. Applications of the compensated spectral natural gamma tool. Paper presented at the 25th ANNUAL SPWLA symposium in New Orleans, June 1984.

Gamma ray spectral data assists in complex formation evaluation. Dresser Atlas, publication REP 06/80 5M 3335, Houston; February 1979.

Hall E, Johnstone CW, Baldwin L, Jacobson LA. A new thermal neutron decay logging system-TDT-M. Paper SPE 9462 presented at the SPE 55th annual technical conference and exhibition, Dallas, Sept. 21-24, 1980; J Petrol Tech. 1982.

Hassan M, Hossin A, Combaz A. Fundamentals of the differential gamma ray log-interpretation technique. Paper presented at the SPWLA 17th annual logging symposium, Denver, June 9-12, 1976.

Herron SL. A total organic carbon log for source rock evaluation. Paper HH, SPWLA symposium. 1986.

Jacobson LA, Ethridge R, Simpson G. A new small-diameter, high-performance reservoir monitoring tool. Halliburton Energy Services.

Kokesh FP. Gamma ray logging. Oil Gas J. 1951.

Marett G, Chevalier P, Souhaite P, Suau J. Shaly sand evaluation using gamma ray spectrometry applied to the North Sea Jurassic. In: SPWLA 17th annual symposium, Denver, June 1976.

McGhee BF, McGuire JA, Vacca HL. Examples of dual spacing thermal neutron decay time logs in Texas Coast oil & gas reservoirs. In: SPWLA Trans. 15th annual logging symposium, June 1974.

Mills Jr WR, Allen S, Caldwell RI, Salaita GN, Gray TJ. Pulsed-neutron experiments in a borehole model. Nucl Sci Eng. 1965;21:346–56.

Murphy RP, Owens WW. The use of special coring and logging procedures for defining reservoir residual oil saturations. J Petrol Tech. 1973:841–50.

Murphy RP, Foster GT, Owens WW. Evaluation of waterfiood residual oil saturations using log-inject-log procedures. J Petrol Tech. 1977:178–86.

Quirein JA, Gardner JS, Watson JT. Combined natural gamma ray spectral-litho-density measurements applied to complex lithologies. Paper SPE 11143 presented at the SPE 57th annual technical conference and exhibition, New Orleans, Sept. 25-29, 1982.

Reed S, Jacobson LA, Durbin D. Cased-hole KUTH logging using a PNS Tool. In: SPE annual technical conference and exhibition, Houston, Texas 26-29 September 2004.

Smith Jr HD, Robbins CA, Arnold DM, Deaton JG. A multi-function compensated spectral natural gamma ray logging system. Paper SPE 12050 presented at the SPE 58th annual technical conference and exhibition, San Francisco, Oct. 5-8, 1983.

Tittman J. “Radiation logging lecture I: physical principle” and “Lecture II: applications”. Petroleum engineering conference on the fundamental theory and quantitative analysis of electric and radioactivity logs, the University of Kansas; 1956.

Wahl JS, Nelligan WB, Frentrop AH, Johnstone, CW, Schwartz RJ. The thermal neutron decay time log. Soc Pet Eng J. 1970:365–37.

Weijun G, Jacobson L, Truax J, Dorffer D, Kwong S. A new three-detector 1-11/16-inch pulsed neutron tool for unconventional reservoirs. In: SPWLA 51st annual logging symposium, Perth, Australia, June 19-23, 2010.

Wiese HC. TDT log applications in California. J Petrol Tech. 1983:429–44.

Youmans AH, Hopkinson EC, Bergan RA, Oshry HI. Neutron lifetime, a new nuclear log. J Petrol Tech. 1964;16:319–28.

Zett A, Webster M, Spain D, Surles D, Colbert C. Application of new generation multi detector pulsed neutron technology in petrophysical surveillance. In: SPWLA 53rd annual logging symposium, June 16-20, 2012.

Zett A, Webster M, Rose H, Riley S, Trcka D, Kadam N. Surveillance of complex displacement mechanisms in mature reservoirs to maximize recovery. In: SPE annual technical conference and exhibition held in San Antonio, Texas, USA 8-10 October, 2012.

Answers to Text Questions

Question #11.1
Uranium

Question #11.2
(c) Σ increase
(d) 30 cu

Question #11.3
$S_w = 50\ \%$

Question #11.5
(a) $\phi = 30\ \%$
(b) $S_w = 50\ \%$
(c) $S_w = 55\ \%$

Question #11.6
$\Sigma_w = 110$ cu

Question #11.7
(a) $\Sigma_{ma} = 13$ cu
(b) $\Sigma_w = 75$ cu

Question #11.8
$\Sigma_o = 21.2$ cu

Question #11.9
Σ methane $= 6.5$ cu
$\Sigma_g = 8.0$ cu

Question #11.10
$\Sigma_{sh} = 33$ cu

Question #11.11
(a) $\phi = 25\ \%$
(b) $\Sigma_{wa} = 50$ cu